RSC Advances

PAPER

View Article Online
View Journal | View Issue

Cite this: *RSC Adv.*, 2024, **14**, 33919

Synergistic antimicrobial nanofiber membranes based on metal incorporated silica nanoparticles as advanced antimicrobial layers†

Piumika Yapa, [a] Imalka Munaweera, *[a] Manjula M. Weerasekera [b] and Laksiri Weerasinghe [a]

In this post-new-normal era, the public prioritizes preventive measures over curing, which is a constructive approach to staying healthy. In this study, an innovative antimicrobial membrane material has been developed, showcasing the promising potential for various applications. The metal-doped silica nanoparticles (Ag, Cu, and Co) were incorporated into a cellulose acetate (CA) polymer-based nanofiber membrane using the electrospinning technique. The metal nanoparticles were doped into a silanol network of silica nanoparticles. The fabricated membranes underwent detailed characterization using a wide range of techniques including PXRD, FTIR, Raman, SEM, TEM, TGA, and tensile testing. These analyses provided compelling evidence confirming the successful incorporation of metal-doped silica nanoparticles (Ag, Cu, and Co) into cellulose-based nanofibers. The band gap energies of the fabricated CA mats lie below 3.00 eV, confirming that they are visible light active. The trimetallic silica nanohybrid exhibited the lowest band gap energy of 2.84 eV, proving the self-sterilizing ability of the CA mats. The DPPH assay further confirmed the best radical scavenging activity by the trimetallic silica nanohybrid incorporated nanofiber mat (91.77 ± 0.88%). The antimicrobial activity was assessed by using the bacterial ATCC strains of *Staphylococcus aureus*, *Streptococcus pneumoniae*, MRSA (Methicillin-resistant *Staphylococcus aureus*), *Escherichia coli*, *Klebsiella pneumoniae*, and *Pseudomonas aeruginosa* and fungal strains; quality control samples of *Trichophyton rubrum*, *Microsporum gypsium*, and *Aspergillus niger*, as well as the ATCC strain of *Candida albicans*. The trimetallic silica nanohybrid-incorporated CA membranes demonstrated the most significant inhibition zones. The reported findings substantiate the self-sterilizing mat's viability, affordability, efficacy against a broad spectrum of microbial strains, cost-effectiveness, and biodegradability. Furthermore, the mat serves as a dual-purpose physical and biological barrier against microbes, affirming its potential impact.

Received 12th July 2024
Accepted 14th October 2024

DOI: 10.1039/d4ra05052e

rsc.li/rsc-advances

1 Introduction

The World Health Organization estimates that each year, 4 million individuals across the European Union contract a medical care-related infection.[1] Despite the fact that certain microorganisms pose no danger to people with good immune systems, proper precautions must be implemented. Hospitals contain a variety of immunocompetent as well as immunosuppressed patients, including patients with immunosuppressors, those who have had infections in the past, and geriatric and pediatric patients.[2,3] Because insufficient or nonexistent measures to prevent infections are in place, public places have additionally been identified as a significant source of infectious disease epidemics. Although the rapid growth of microorganisms as well as the ensuing spread of infections is a major global concern, there are currently very few laws or regulations in place to restrict the spread of infections in public areas.[4,5]

Nevertheless, it is crucial to take preventive measures without wasting time implementing policies and relevant guidelines on this matter. Self-sterilizing materials have the special ability to reduce the number of pathogenic microbes that are brought into contact with them by causing redox stress and destroying the microbial cells by photothermally, photocatalytically, or chemical reactions.[6,7] These materials show significant promise in the fight against the spreading of numerous infections, especially those produced by aerosolized droplets that are infected and spread from an individual to nearby counterparts. The goal of covering inanimate objects with antimicrobial compounds that possess a self-sterilizing

[a]*Department of Chemistry, Faculty of Applied Sciences, University of Sri Jayewardenepura, Nugegoda, 10250, Sri Lanka. E-mail: imalka@sjp.ac.lk; laksiri@sjp.ac.lk; piumikayapa@gmail.com; Tel: +94 772943738*

[b]*Department of Microbiology, Faculty of Medical Sciences, University of Sri Jayewardenepura, Nugegoda, 10250, Sri Lanka. E-mail: mmweera@sjp.ac.lk*

† Electronic supplementary information (ESI) available. See DOI: https://doi.org/10.1039/d4ra05052e

ability is to hinder the microbes from spreading by shortening their life span, destroying them structurally, or interfering with their physiology, which restricts the microbes from multiplying, growing, and spreading. When coated on interfaces as thin films, self-cleaning materials show bactericidal and fungicidal effectiveness by inducing oxidative stress, which ultimately kills the microbial cells.[8,9]

Sustainable polymeric matrices with antimicrobial capabilities as self-sterilizing materials are presently highly sought after for applications in medicine, including personal protective equipment (PPE), medical robes, bed linens, and other medical apparel used in healthcare settings[10,11] as well as daily use by healthy individuals, in order to sustain the highest possible standards of public health. This effort obeys the concept that "prevention is better than cure".[12] However, with the unprecedented demands of PPE in these infectious environments, the supply of PPE has become inadequate all over the world due to the inefficient supply, high prices, and expensive and sophisticated technologies that are used to fabricate PPE.[13,14] Personal hygiene products such as women's sanitary napkins, baby diapers, and adult diapers play a significant role, as does PPE when focusing on public health.[15] Microbial infections and several dermal problems arising from the microbes are the predominant issues with these personal hygiene products.[16–18] The World Health Organization (WHO) highlights the importance of menstrual health among women and the good quality of geriatric life through promising protection against microbes when using hygiene products.[19] Therefore, simple, efficient, and affordable personal hygiene products with promising microbial action should be available to fulfill the demands and expectations for personal hygiene products among the global public.[20–23] The most recent suggestions include surfaces with anti-adhesive qualities, antibacterial chemicals integrated into the surface, or surfaces modified with biologically active metals.[24–26]

Recently, "nanoantibiotics"—nanostructures with particle sizes between 1 and 100 nanometers—have emerged as new antibacterial agents. Several investigations have demonstrated that nanomaterials have stronger antibacterial effects against both Gram-positive and Gram-negative bacteria. The WHO also accepted this concept as a solution for Multi-Drug Resistance (MDR) of microbes because metal nanoparticles have a well-proven antimicrobial action against a broad spectrum of microbes.[27] Its nanoscale dimension enables it to have better features, which have helped it reach several important milestones in applications in biology and medicine.[28–32]

A new phase in medicine was ushered in by the discovery of metallic nanoparticles along with their prospects for therapeutic applications.[33] The strong antimicrobial properties they have exhibited against a range of microbes have taken scientists from all around the world by astonishment.[34–36] By combining two or more metallic nanoparticles, synergistic strategies deliver greater efficacy than any of the individual components might. It is preferable to follow synergistic strategies to span an extensive range of bacteria as well as others.[37,38] The doping of metallic nanoparticles into a cargo loading agent such as silica offers many benefits, such as the synergistic activity of the overall system of nanohybrids, the precisely controlled installation of various metals resulting in a homogeneous distribution, and the stabilization of particular metals within the structures that avoid accumulation during consumption.[39–41]

In this study, we have developed and characterized multi-metallic silica nanohybrids loaded polymer-based membranes that are associated with antimicrobial activity. It has the potential to be readily used as an antimicrobial functional layer in personal protection equipment, and personal hygiene products. The antimicrobial functional layer is fabricated with the novel technology "electrospinning" by using biodegradable, eco-friendly, apparently nontoxic polymer. On the contrary, synthetic polymer membranes lead to several issues, including high cost, irritability, non-biodegradability, *etc.* Due to the multifaceted porous framework, extremely efficient surface area, and flexibility during use, electrospun nanofiber was originally thought to be the most suitable option for immobilizing these nanohybrids on a suitable solid inert substrate with the desired morphological configuration.[42] Electrospinning is a straightforward, recently developed method for generating ultrathin fibers with nanoscale dimensions by using electrostatic forces. Compared to other methods, electrospinning yields membranes with a higher surface area-to-volume ratio. Additionally, the electrospun nanofiber membrane guarantees the reusable nature of the integrated antimicrobial agents because of their fibrous arrangement, making it difficult to separate the powdered nanohybrids from the fibrous network.[43]

In this study, the non-woven cellulose acetate electrospun membrane consists of nanofibers and acts as a matrix for the incorporated silver (Ag), copper (Cu), and cobalt (Co)-doped mesoporous silica nanohybrids. In our prior research, we thoroughly examined the combined antimicrobial effects of a metallic silica nanohybrid against an extensive array of microorganisms, revealing its potential to combat a wide spectrum of microbial threats.[44,45] This study serves as a vital extension of our prior research, significantly enabling the practical application of multi-metallic silica nanohybrids loaded electrospun polymer-based membranes as active antibacterials layers. Fig. 1 shows a graphical illustration of the research approach.

When considering recent research publications, Abdelgawad *et al.*[46] reported the feasibility of generating nanofibrous chitosan/polyvinyl alcohol (PVOH) fibers with the inclusion of AgNPs. According to the results of the antibacterial evaluation, these fibers exhibited adequate resistance against *E. coli*, and bacterial mortality decreased as the chitosan content increased. Abrigo *et al.*[47] have also reported an advanced biomedical device with two layers made of electrospun chitosan/TiO_2 fibers. Because of the synergistic interaction between chitosan and TiO_2, these intriguing materials demonstrated a relatively small amount of bacterial penetration (*E. coli* and *S. aureus*). According to our knowledge, this study will be the first research that proves an antimicrobial activity against an extensive spectrum of microbes. Therefore, this product would establish the availability of universal and equitable access to an antimicrobial functional layer against tested pathogens.[48–50]

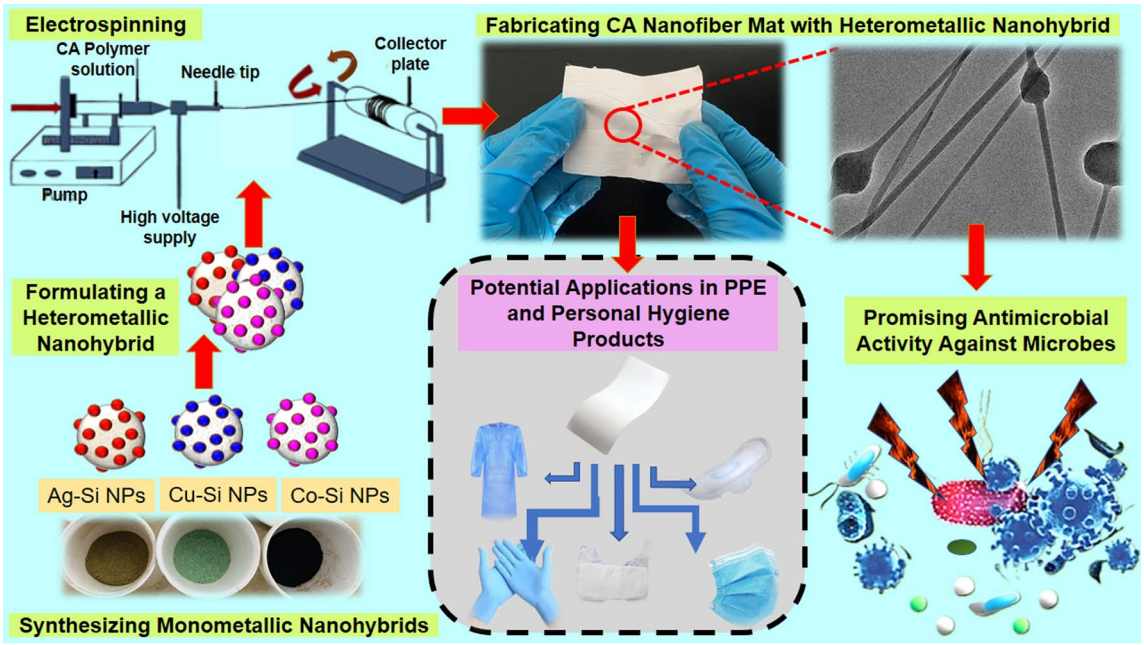

Fig. 1 A graphical illustration of the research approach.

Personal Protection Equipment (PPE) and personal hygiene products can be reinforced with conventional antibiotics to diminish infectious diseases; however, antibiotic resistance, affordability, and availability are some questionable areas. Therefore, this invented multimetallic silica based nanohybrids, which is readily incorporated into the cellulose acetate membranes, ensures availability, affordability, activity against resistant strains and a broad spectrum of microbes, cost-effectiveness, and acts as both a physical and biological barrier. Additionally, this invented antimicrobial electrospun membrane is apparently nontoxic, and it is biodegradable with minimum hazards to the environment.

2 Materials and methods

2.1 Materials

Analytical-grade 2,2 diphenyl-1-picrylhydrazyl (DPPH), methanol, ascorbic acid, acetone, dimethylformamide, cellulose acetate, barium chloride ($BaCl_2$), and sulfuric acid (H_2SO_4) were purchased from Sigma-Aldrich in the United States. HiMedia in India provided the analytical-grade chemicals, media, and other materials needed for microbiology research, including nutritional agar, Muller Hinton agar, bacteriological agar, Sabouraud dextrose agar, blood agar, and antibiotic discs.

For microbiology studies, the bacterial strains (ATCC cultures and clinical isolates) of *Staphylococcus aureus* (ATCC 25923), *Streptococcus pneumonia* (ATCC 49619), MRSA (Methicillin-resistant *Staphylococcus aureus*), *Escherichia coli* (ATCC 25922), *Klebsiella pneumonia* (ATCC BAA 1706), and *Pseudomonas aeruginosa* (ATCC 27853) and fungal strains; quality control samples of *Trichophyton rubrum*, *Microsporum gypsium*, and *Aspergillus niger*, as well as the ATCC strain of *Candida albicans* (ATCC 10231), the clinical isolates of these fungi were obtained from the Department of Microbiology at the University of Sri Jayewardenepura in Sri Lanka.

2.2 Methodology

2.2.1 Fabrication of heterometallic silica nanohybrids incorporated polymer-based electrospun nanofiber membranes. Trimetallic silica nanohybrids were synthesized in accordance with the methodology outlined in our previous work.[44,45] Cellulose acetate (CA), with a molecular weight of 100 kDa, was used as the polymer to fabricate the electrospun membrane by incorporating the synthesized metallic silica nanohybrids. In this study, five types of electrospun membranes were fabricated, including the CA-only mat (CA-mat), CA-mat loaded with 50% (w/w) of Ag-doped silica nanohybrid (Ag-Si-CA), CA-mat loaded with 50% (w/w) of Cu-doped silica nanohybrid (Cu-Si-CA), CA-mat loaded with 50% (w/w) of Co-doped silica nanohybrid (Co-Si-CA), and finally CA-mat loaded with 50% (w/w) trimetallic silica nanohybrid (Ag-doped silica nanohybrid + Cu-doped silica nanohybrid + Co-doped silica nanohybrid) (Ag-Si + Cu-Si + Co-Si-CA). These membranes were denoted as CA-mat, Ag–Si-CA-mat, Cu–Si-CA-mat, Co-Si-CA-mat, and Ag-Si + Cu-Si + Co-Si-CA-mat respectively hereafter.

To obtain the CA-mat, 600 mg of cellulose acetate (100 kDa) was added to a solvent mixture of acetone and DMF (2 : 1 v/v). The resulting solution was subsequently introduced into a syringe with a blunt-ended needle. Then, a layer of aluminium foil was laid out over the ground collector plate to capture the fibers. The solution involved electrospinning using a static collector plate along with an SKE EF100 electrospinning system under ambient room temperature and humidity, using a voltage of 16 kV, a tip-to-collector distance of 13 cm, and a rate of flow of 1.5 mL h^{-1}.[51]

In the case of fabricating the metallic silica nanohybrids incorporated CA-mats, the polymer solution was prepared as before, and 600 mg of the respective metallic silica nanohybrid was incorporated into the prepared CA polymer solution. Then the solution was sonicated for 5 hours at room temperature. The resulting solution was subjected to electrospinning as described previously by applying the same parameters.[52]

2.2.2 Characterization of metallic silica nanohybrids incorporated electrospun CA mats. The CA-mat and the nanohybrids incorporated CA-mats have been examined using Raman spectroscopy (Model-Thermo Scientific DXR with fine power of laser, the range −500–2500 cm^{-1} as well as Fourier transform infrared (FTIR) analysis – ATR mode (Bruker Vertex 80 instrument) across the range of 400 cm^{-1} to 4000 cm^{-1} to analyze the functional groups of the materials. Utilizing the software entitled SmartLab Studio II, the crystal phase of the heterometallic silica nanohybrid have been studied using X-ray diffraction (XRD) analysis (Rigaku smart lab, 3 kW sealed X-ray tube) in the range of 5–85, two theta degree range.[45]

Employing transmission electron microscopy (TEM), model – JEOL JEM-2100, that is operated at a voltage of 20 kV as well as scanning electron microscopy (SEM), model – ZEISS model, method of secondary electron, using an accelerated voltage of 10 kV, the morphological features of metallic silica nanohybrids incorporated electrospun nanofiber mats were examined. The fiber diameter and the distribution of the fiber diameter of the fabricated mats have been calculated using Image J software (Image J 1.51). The composition of each metallic nanohybrids and the homogenous distribution in the fabricated nanofiber mats were confirmed *via* atomic absorption spectrometry (AAS) analysis (Thermo Scientific iCE 3000 model).[45,53,54] Before performing the AAS analysis, metallic silica nanohybrids incorporated nanofiber mats were digested according to the method described by Uddin *et al.*[55]

2.2.3 Evaluating the band gap energies of the fabricated nanofiber mats. The optical band gap energies (E_g) of the silica nanohybrid incorporated CA-mats were determined using UV-vis diffuse reflectance spectrometry. The band gaps of each CA-mat were determined by extrapolating the linear portion of the plot to $(F(R)h\nu)^2 = 0$.[56,57]

From the fabricated Ag-Si + Cu-Si + Co-Si-CA-mat which holds an area of 121 cm^2 (11 × 11 cm), samples were taken at five different places. Then these samples were tested for their band gap energies. The evaluated band gap energies were compared to confirm the homogeneity of the band gap energies of the materials at any place of the Ag-Si + Cu-Si + Co-Si-CA-mat.

2.2.4 Digestion of metallic silica nanohybrids incorporated nanofiber mats to determine the composition of each metal in a unit area. To confirm the homogenous distribution of each metal throughout the metallic silica nanohybrids incorporated nanofiber mat (121 cm^2 (11 cm × 11 cm)), an atomic absorption spectroscopy investigation was conducted. The following process was used to manually digest the samples of electrospun nanofiber mats before their analysis. In a distinct boiling tube, 1 cm^2 of each sample was treated with a 10 mL mixture of HCl and HNO_3 acids (3 : 1). The resulting mixture was heated at 90 °C for 4 hours,[55] allowed to cool to an ambient temperature, filtered, and then the AAS analysis was performed.

2.2.5 AAS analysis of metallic silica nanohybrids incorporated nanofiber mats to confirm the homogeneity of the metal distribution. From each of the fabricated nanofiber mats, with an area of 1 cm^2, samples were taken at five different places. These samples were digested manually, as described in Section 2.2.4. Then the digested samples were subjected to AAS analysis, to determine the composition of each metal at the respective places of the mat. Each composition was compared, to confirm the distribution and the homogeneity of each metal in the respective area in the nanofiber mat statistically. The test was triplicated for statistical validity.[45]

2.2.6 DPPH assay for evaluating the radical scavenging activity of metallic silica nanohybrids incorporated nanofiber mats. The radical-scavenging potential associated with the metallic silica nanohybrids incorporated nanofiber mats has been assessed by employing DPPH as a free radical material. The UV-vis spectra were obtained using UV-VIS spectroscopy, model – PerkinElmer, LAMBDA 365+ double beam in accordance with a method described by Sanna *et al.*[58] Methanol and DPPH were used in the UV-VIS tests. After 30 minutes of magnetic stirring in the dark, the 0.1 mM DPPH solution was ready to be used in the DPPH assay. A test tube has been filled with a 0.5 cm^2 section of membrane, 1 mL of distilled water, along with 1 mL of 0.1 mM of prepared DPPH solution. After shaking the entire mixture well, the absorbance at a wavelength of 517 nm was measured after 30 minutes. The following formula was used in order to determine the percentage that represents DPPH degradation. Employing distinct sections of the fiber membranes, the study was performed three times for each mat.

$$\text{DPPH scavenging activity} = \frac{A_0 - A_1}{A_0} \times 100\%$$

where A_0 and A_1 represent the respective absorbance of each sample of nanofiber mat without and with exposure to DPPH.[45]

2.2.7 Evaluation of the antimicrobial activity of the metallic silica nanohybrids incorporated nanofiber mats. As the minimum inhibitory concentration (MIC), minimum bactericidal concentration (MBC), and minimum fungicidal concentration (MFC) of the incorporated metallic silica nanohybrids were previously reported in our previous detailed study,[44,45] the disc diffusion method was carried out to investigate the antimicrobial activity of the metallic silica nanohybrids incorporated nanofiber mats. Ag-Si-CA-mat, Cu-Si-CA-mat, Co-Si-CA-mat, and Ag-Si + Cu-Si + Co-Si-CA-mat were tested against the ATCC cultures of Gram-positive bacteria; *Staphylococcus aureus* (ATCC 25923), *Streptococcus pneumoniae* (ATCC 49619), methicillin-resistant *Staphylococcus aureus* (MRSA); Gram-negative bacteria; *Escherichia coli* (ATCC 25922), *Klebsiella pneumoniae* (ATCC BAA 1706), and *Pseudomonas aeruginosa* (ATCC 27853) and fungi; quality control samples of *Trichophyton rubrum, Microsporum gypsium*, and *Aspergillus niger*, as well as the ATCC strain of *Candida albicans* (ATCC 10231). Erythromycin (15 μg) was used as the positive control for Gram-positive bacteria. Gentamycin (15 μg) was used for *P. aureginosa*, *K.*

pneumoniae, and *E. coli.* Fluconazole (15 μg) was used as the positive control for fungi. A disc of CA-mat was used as the negative control.

The disposable micropipette tips as well as the media were autoclaved for 15 minutes at 121 °C and 15 bar of pressure. Other equipment made of glass was sterilized for two hours at 160 °C in a hot air furnace. Each expendable Petri plate was filled with 25 mL of agar medium (MHA for bacteria and SDA for fungi), which was then left to solidify. Subsequently, 3 mL of the microbial suspensions, standardized to 0.5 McFarland's standard (10^8 CFU mL^{-1}), were applied over the agar medium's surface. The previously described microbial strains were used for producing microbial suspensions. The surplus solution was eliminated once the suspension had been evenly applied throughout the agar surface. Then the prepared discs were placed on the agar surface by using sterile forceps. Each plate was incubated at 37 °C for 24 hours. Next, using a Netillin Zone Reader (USA), the zone of inhibition over every disc was calculated.[45] Every technique was carried out in triplicate in compliance with CLSI recommendations,[59] M 27 guidelines[60] for yeast – *C. albicans*.

Although there are numerous studies that have been published in high-impacted journals using disc diffusion assays over filamentous fungi including *A. niger*, *M. gypseum*, and *T. rubrum*, the assay is typically not advised as a regular procedure for these kinds of fungi. Therefore, for the purpose of verifying the antifungal activity of the fabricated nanofiber mats, we also performed a disc diffusion assay for the chosen filamentous fungus in this case.[61–63] The previously indicated process was further carried out for the clinical isolates of all the microbial strains. For each microbial strain, five clinical isolates ($N = 5$) were evaluated.[45]

2.2.8 Scanning electron microscopy (SEM) analysis of microbial cultures after treating with the trimetallic silica nanohybrid incorporated CA nanofiber mats. To examine the structural alterations of microbes when exposed to the fabricated metallic silica nanohybrids incorporated in nanofiber mats, SEM examination was performed. After the well diffusion assay was performed as described in Section 2.2.7, the discs of CA only mat (negative control) and the disc of the trimetallic silica nanohybrid incorporated nanofiber mat were taken out and subjected to the SEM imaging. This imaging was carried out for all the selected ATCC strains of bacteria including *Staphylococcus aureus*, *Streptococcus pneumoniae*, MRSA (Methicillin-resistant *Staphylococcus aureus*), *Escherichia coli*, *Klebsiella pneumoniae*, and *Pseudomonas aeruginosa* and fungal strains; quality control samples of *Trichophyton rubrum*, *Microsporum gypsium*, and *Aspergillus niger*, as well as the ATCC strain of *Candida albicans*.[64]

2.2.9 Thermal and mechanical properties of electrospun CA-mat and trimetallic silica nanohybrids incorpertaed CA-mat. The thermal and mechanochemical stability of fibers plays a pivotal role in acting as a reinforcing agent, particularly considering the processing temperatures they encounter. The thermal decomposition behavior of the cellulose acetate mat and trimetallic silica nanohybrid incorporated cellulose acetate mat were investigated using TGA and the first derivative curve (DTGA), (TGA SDT 650-discovery series) in the temperature range of 27–320 °C by using the Ramp 1 °C min^{-1}.[65,66] The tensile strength of the electrospun mats was determined by the tensile strength tester, Instron 3365 model, and the software Bluehill lite, version 2.32. The load cell that was used for the tensile strength test was 100 N. The thickness of the CA mats was determined by the thickness meter – Wallace test equipment.[67,68]

2.2.10 Leach-out experiment of the trimetallic silica nanohybrid incorporated CA-mat. The leaching-out experiment was carried out for the fabricated Ag-Si + Cu-Si + Co-Si-CA-mat that exhibits the best antimicrobial potential to confirm that there is no leaching-out effect of incorporated metallic silica nanohybrids. The experiment was carried out for Ag-Si + Cu-Si + Co-Si-CA-mat. Firstly, nutrient broth agar media was prepared, and 5 mL of the prepared media was poured into sterile centrifuge tubes. Then 1 mL of freshly prepared microbial culture of *S. aureus*, which was compared with Mcfarland standard, was introduced to each centrifuge tube separately. An area of 25 cm^2 (5 cm × 5 cm) from the trimetallic silica nanohybrid incorporated CA-mat was taken and immersed in the prepared samples. Then the samples were incubated for a defined incubation period (24 hours). Then the solution was subjected to IC-PMS analysis at the detection level of 1 ppb to investigate the metal (Ag, Cu, and Co) concentrations in the solution and to confirm whether there is any leach out of metallic nanoparticles from the CA-nanofibers.

2.2.11 Electrospinning trimetallic silica nanohybrid incorporated CA nanofiber on the surface of a commercially available diaper as a practical implementation. After comparing the antimicrobial activity of monometallic silica nanohybrid incorporated nanofiber mats and the trimetallic silica nanohybrid incorporated nanofiber mat, the best-performing nanofiber mat was chosen for this purpose. The polymer solution of the best-performing nanofiber mat was prepared and subjected to electrospinning on the surface of a diaper using the same parameters described in Section 2.2.1. The resulting membrane, along with the diaper, was analyzed by using SEM imaging to investigate the morphological characteristics.

2.2.12 Evaluation of the antimicrobial activity of the electrospun nanofiber mat on the surface of the diaper. The disc diffusion assay was performed to assess the antimicrobial activity of the electrospun nanofiber mat on the surface of the diaper. A disc of the commercially available diaper was used as the negative control. The positive control was a standard antibiotic that was selected according to the strain of the microorganism, as in 2.2.7. Six other discs from the electrospun nanofiber mat on the surface of the diaper were used. These discs, excluding the positive control, were prepared by soaking the discs in artificial urine that was prepared according to the method.[69] The discs were taken out from the prepared solution of artificial urine in different time durations; 2, 4, 8, 16, and 24 hours (proper side of the exposed mat), and 24 hours (upside down side of the exposed mat) and placed on the agar surface of the prepared Petri dishes with selected strains of microbes. These discs were investigated for their antimicrobial activity

against the previously selected strains of microbes as decribes in 2.2.7.

2.2.13 Statistical analysis. A one-way analysis of variance (ANOVA) was used to assess the significance difference amongst the means following the calculation of the incorporated compositions of each metal into the nanofiber mat, with a significance level of $P < 0.05$. The Tukey pairwise comparison analysis followed next. After a comprehensive statistical study confirmed that there is no substantial difference between the composition of each metal at the selected places, representing the whole area of the nanofiber mat where the antimicrobial assays by disc diffusion were carried out. This was performed by considering that the metal distribution is homogenous all over the mat based on the above results.

The mean value of the zones of inhibition displayed by each metallic silica nanohybrid incorporated nanofiber mat against all the chosen microbial strains (both ATCC and clinical isolates) was then statistically analyzed using a 2-sample *t*-test. We employed a significance threshold of $P < 0.05$.

To confirm that the antimicrobial action of the electrospun nanofiber mat on the diaper surface does not fluctuate with time, a one-way analysis of variance (ANOVA) was performed. This is to assess the significance difference amongst the means of the zones of inhibition of each disc at different time durations (up to 24 hours).[45]

3 Results and discussion

An electrospun nanofiber mat with antibacterial properties was developed in this research. As an antimicrobial functional layer, it can be easily incorporated into various personal hygiene products, such as baby and adult diapers, sanitary napkins, and other PPE. A unique process called "electrospinning" is used to create the antimicrobial functional layer using cellulose acetate (CA). CA, a biodegradable and environmentally beneficial polymer, and it is reportedly harmless. This non-woven membrane consists of nanofibers that act as a matrix for the incorporated Ag, Cu, and Co-silica nanohybrids. These metals are well-proven for their antimicrobial properties when employed separately. Here, a synergistic antimicrobial activity was obtained by combining all these silica nanohybrids in a common matrix and this product would establish the availability of universal and equitable access to an antimicrobial functional layer against infectious diseases.[45,69,70] Although this is a continuation of a previous study that discusses the antibacterial and antifungal activity of multimetallic nanohybrids by the same group of authors, here it is explained a novel practical approach of incorporating the multimetallic nanohybrids into polymer matrices. The characterization and evaluation of the antimicrobial potential of the innovated polymer-based nanofibrous mats will be discussed here.

3.1 Characterization of fabricated CA electrospun mats containing metallic silica nanohybrids (50% w/w)

The nanofiber mats produced through electrospinning can be easily separated from the aluminum foil collector and exhibit a uniform texture, appearing as a white mat. These nanofiber mats were then characterized structurally and morphologically. First, XRD analysis was conducted to confirm the successful incorporation of metallic silica nanohybrids into the cellulose acetate (CA) nanofiber mat during the process of electrospinning. Fig. 2(a) shows the X-ray diffractograms of CA-mats in comparison with monometallic silica nanohybrids incorporated CA-mats and trimetallic silica nanohybrids incorporated CA-mats. CA is a derivative of cellulose that is insoluble in water as well as amorphous in nature. Consequently, the absence of distinct and intense peaks associated with CA was noted. Broad peaks were observed within the range of 15–30 theta degrees, which are indicative of the presence of CA.[71–74] These peaks were depicted in a square in Fig. 2(a)(i–v). The low intensity of these peaks can be attributed to the amorphous nature of the material.

A comparison was made between the X-ray diffractogram of CA and the fabricated nanofiber mats that were incorporated with metallic silica nanohybrids. The X-ray diffractogram of the Ag-Si-CA-mat, as shown in Fig. 2(a-ii), exhibits distinct peaks that correspond to the Ag–O bond. The Miller indices 111, 200, 220, and 311 can be employed to distinguish face-centered cubic (fcc) silver based on the well-defined diffraction peaks observed at 2θ values within the 5–85° range. The presence of these peaks confirms the crystalline structure of AgO. The observed peaks correspond to the AgO crystalline structure as reported in the JCPDS file with reference number 04-0783.[45,69–71] A broad peak between 25 and 30° that is quite faintly intense indicates that amorphous silica is present in the sample. In Fig. 2(a-iii), the X-ray diffractogram of Cu-Si-CA-mat depicts peaks that govern for Cu–O. The miller indices −111, −112, 220, and 311 can be used to index the well-resolved diffraction peaks at 2θ values in the range of 15–85° to cubic copper. These peaks attest to CuO's crystalline structure. CuO crystalline structure is allocated to JCPDS file no. 05-0661, whereby the resolved peaks correspond well with the fabricated material.[45,69–71] This spectrum also shows the broad peak, which is relatively low in intensity, between two theta 25–30. It attests to the amorphous silica composition in the sample.

Fig. 2(a-iv) shows the X-ray diffractogram of the Co-Si-CA-mat that depicts peaks that govern for Co–O.[66] A number of well-resolved diffraction peaks at 2θ values in the range of 15–85° can be indexed to cubic cobalt oxide (Co_3O_4) with miller indices 220, 311, 400, 511, and 440. These peaks confirm the crystalline structure of Co_3O_4. The resolved peaks are well-matched with JCPDS file no. 42-1467 (Co_3O_4), which is assigned to Cu–O crystalline structures. Fig. 2(a-v) shows the X-ray diffractogram of Ag-Si + Cu-Si + Co-Si-CA-mat that depicts peaks which govern for Ag–O, Cu–O, and Co–O. However, all the peaks that were associated with each metallic crystalline structure (Fig. 2(a)(ii–iv)) cannot be clearly observed in the PXRD pattern Fig. 2(a-v) due to the amorphous nature of the cellulose acetate electrospun membranes (Fig. 2(a-i)). The presence of crystalline structures inside an amorphous polymer matrix composed of CA may impede the detection of low-intensity peaks. However, there were some well-resolved peaks that govern the three metals and these peaks indicated the presence of the three

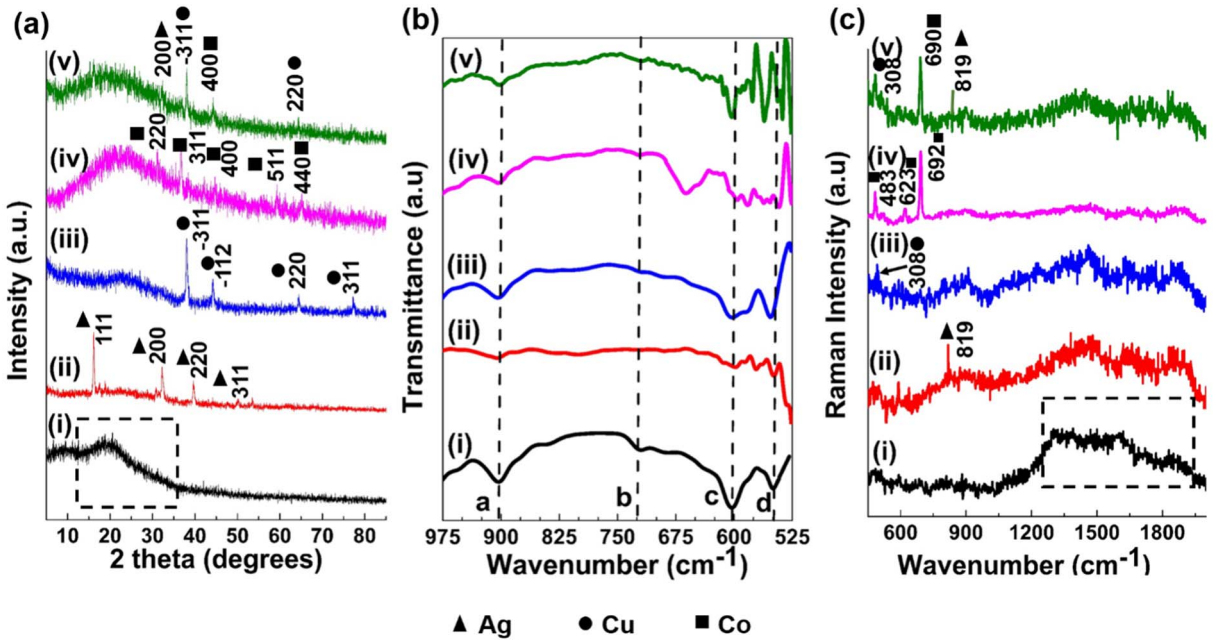

Fig. 2 (a) The XRD analysis, (b) the FT-IR analysis, and (c) the Raman analysis of; (i) CA-mat, (ii) Ag-Si-CA-mat, (iii) Cu-Si-CA-mat, (iv) Co-Si-CA-mat, (v) Ag-Si + Cu-Si + Co-Si-CA-mat.

metallic silica nanohybrids in the CA-mat. As observed the peaks with the miller indices 200 govern for Ag–O, −311 and 220 govern for Cu–O, and 400 govern for Co–O crystalline structures.

Subsequently, to provide evidence of the creation and modification of particular chemical interactions in the fabricated nanofiber mats, FT-IR analysis was conducted using ATR mode within the wavelength range of 500–4000 cm^{-1}. The bond vibrations and peak shifts were comprehensively examined by obtaining the FT-IR spectra within the fingerprint region (950–500 cm^{-1}).

Furthermore, a comparison was carried out to compare the relevant peak positions that govern the bond vibrations between the CA-mat and the metallic silica nanohybrid included CA-mat (Fig. 2(b)). The bond vibrations of CA are governed by four different peaks. These peaks are labeled as a–d in all FTIR spectra. The peak that is labeled "a" at 904 cm^{-1} governs C–CH_3 bending, the peak that is labeled "b" at 721 cm^{-1} governs =C–H bending, the peak that is labeled "c" at 603 cm^{-1} governs –C–H_3 and the peak that is labeled "d" at 551 cm^{-1} governs C–H out of plane vibrations. Fig. 2 (b-i) depicts the FTIR spectra of CA-mat, Fig. 2(b-ii) depicts the FTIR spectra of Ag-Si-CA-mat, Fig. 2(b-iii) depicts the FTIR spectra of Cu-Si-CA-mat, Fig. 2(b-iv) depicts the FTIR spectra of Co-Si-CA-mat and Fig. 2(b-v) depicts the FTIR spectra of Ag-Si + Cu-Si + Co-Si-CA-mat. The presence of metallic silica nanohybrids in the CA polymer matrix has caused the labeled peaks of a, b, c, and d in these spectra to shift to the left and right due to the electrostatic interactions.[73–76] The relevant peak shifts in each spectrum are displayed in Table 1.

Raman analysis was performed to further evaluate the bond vibrations and peak shifts in these developed metal nanohybrids incorporated CA-mats. Fig. 2(c) depicts the Raman spectra of all the fabricated CA-mats. In all the spectra, it can be clearly observed that there is a cluster of peaks in the range of 1150–1900 cm^{-1} (denoted within a dash lined square) that govern bond vibrations in CA. These peaks have lowered their intensity in a significant manner in all the spectra of metallic silica nanohybrid incorporated CA-mats due to the incorporation of metallic silica nanohybrids into the CA-mat. Fig. 2(c-i) shows the Raman spectra of the CA-mat, Fig. 2(c-ii) Ag-Si-CA-mat. The peak at 819 cm^{-1} governs Ag–O bond vibrations. Fig. 2(c-iii) shows the Raman spectra of Cu-Si-CA-mat. The peak at 308 cm^{-1} governs Cu–O bond vibrations. Fig. 2(c-iv) shows the Raman spectra of the Co-Si-CA-mat. The peaks at 483, 623, and 692 cm^{-1} govern for Co–O bond vibrations. Fig. 2(c-v) shows the Raman spectra of Ag-Si + Cu-Si + Co-Si-CA-mat. The peaks at 819 cm^{-1} and 308 cm^{-1} govern Ag–O, and Cu–O bond vibrations respectively. Peaks at 484 and 690 cm^{-1} govern the Co–O bond vibrations. These peaks clearly indicate the presence of metallic silica nanohybrids within the CA polymer matrix. These four spectra did not show all the peaks govern for all the bond vibrations that are responsible for metal–oxygen bonds. The reason behind this can be the low-intensity peaks may be hindered because these crystalline structures were embedded in an amorphous polymer matrix made of CA.[66–71,77]

After the structural characterization, the fabricated nanofiber mats were morphologically analyzed by SEM and TEM imaging. As depicted in Fig. 3, it is well proven the successful incorporation of metallic silica nanohybrids into the CA-matrix.[44,45]

When analyzing these SEM and TEM images, it is evident that the addition of metallic silica nanohybrids has decreased fiber diameter. The total electrical charge of the electrospinning

Table 1 The peak positions and relevant bond vibrations of metallic silica nanohybrids incorporated electrospun membranes at the range 500 to 950 cm^{-1}

Assigned to	Bond vibration	CA-mat (cm^{-1})	Ag-Si-CA-mat (cm^{-1})	Cu-Si-CA-mat (cm^{-1})	Co-Si-CA-mat (cm^{-1})	Ag-Si + Cu-Si + Co-Si-CA-mat (cm^{-1})
a	C–CH_3 bending	904	906	906	904	902
b	=C–H bending	721	742	719	721	725
c	=C–H	603	597	601	662	604
d	C–H out of plane	551	542	562	561	546
O–Si–O	O–Si–O	—	829	799	798	798
			800			
Ag–O	Ag–O	—	689	—	—	688
Ag–O	Ag–O	—	571	—	—	571
Cu–O	Cu–O	—	—	562	—	562
Co–O	Co–O	—	—	—	645	644
Co–O	Co–O	—	—	—	595	596
Co–O	Co–O	—	—	—	582	582
Co–O	Co–O	—	—	—	561	563

jet surged dramatically with the incorporation of metallic silica nanohybrids, which also caused a larger charge density to accumulate on the outermost layer of the ejected jet within the process.[78] Greater elongation forces that might surpass the self-repulsion were transmitted down to the jet underneath the electric field that formed as the jet's charges rose. As a result, the diameter of the fibers shrank as the charge density rose.[79]

This will be advantageous because, when the fiber diameter is decreased, the penetration ability of visible light to the nanofiber mat is increased. Visible light governs the activation and initiation of ROS from the metallic nanoparticles that give rise to the antimicrobial potential.[80,81] The software Image J was then used to determine the mean diameter of the fibers to gain insight into the distribution of fiber diameter. The mean diameters of the fibers were 119, 30, 41, 41, and 30 nm that belong to CA-mat, Ag-Si-CA-mat, Cu-Si-CA-mat, Co-Si-CA-mat and Ag-Si + Cu-Si + Co-Si-CA-mat respectively.

3.2 Evaluating the band gap energy, thermal and mechanical properties of metallic silica nanohybrids incorporated CA-mats

The optical band gap energy (E_g) of the trimetallic silica nanohybrid incorporated cellulose acetate nanofiber mat (Fig. 4(a)) was determined using UV-vis diffuse reflectance spectrometry. Monometallic silica nanohybrids incorporated nanofiber mats include Ag-Si-CA-mat incorporated nanofiber mat, Cu-Si-CA-mat, and Co-Si-CA-mat. Trimetallic silica nanohybrids incorporated nanofiber mats include Ag-Si + Cu-Si + Co-Si-CA-mat. The band gaps of each sample were determined by extrapolating the linear portion of the plot to the $(F(R)h\nu)^2 = 0$ axis. Table 2 shows the respective band gap energy of each nanofiber mat. ESI data† file 01 shows the band gap energies of monometallic and trimetallic silica nanohybrids incorporated in nanofiber mats.[56,57]

According to the reported results, the band gap of all the nanofiber mats lies in the range of 2.84–2.92 eV in the visible light region enabling it to act as a visible light active photocatalytic material. The trimetallic silica nanohybrid incorporated CA-mat exhibited the lowest band gap energy 2.84 eV in the visible light region compared to the monometallic silica nanohybrid incorporated nanofiber mats and exhibited good photocatalytic activity under visible light. Owing to their semiconducting attributes, metallic nanoparticles are a widely used class of nanomaterials in various industries. They are generated in large quantities and are often employed as catalysts for redox reactions in both artificial and natural settings.[82] Not only might metallic nanoparticles function as channels for the transfer of electrons between aqueous reactants, although the transfer of electrons is also contingent upon the energy states of the nanomaterials alongside the redox-active aqueous materials being identical. Considering the recorded results here, it is well proven that all the fabricated electrospun membranes incorporated with metallic nanohybrids are active under visible light, with the multimetallic silica nanohybrid demonstrating the lowest band gap energy at 2.84 eV, affirming its self-sterilizing capability. These results are in good agreement with the recently published data as well. Tzevelekidis *et al.* have reported nanohybrids comprised of Cu-doped and Ag-decorated TiO_2, that exhibit antibacterial activity against *S. aureus* and *E. coli*.[83] Similarly, Matalkeh *et al.* have reported on an antimicrobial activity of nanocrystalline silver (Ag), supported by tungsten oxide (WO_3) against Gram-positive and Gram-negative bacteria under visible light.[84]

Moreover, Burello and Worth[85] proposed a theoretical paradigm that explains how some of these materials cause oxidative stress and toxicity by relating the band gap of metallic nanoparticles to the cellular redox potential. Thus, permissive electron transfers may result in the generation of oxidizing or reducing materials that lower the amount of antioxidants and/or increase the generation of reactive oxygen species (ROS) and/or oxidized biological components while the biological and material energetic states are identical.

The generation of ROS is the main mechanism which governs the antimicrobial activity of metallic nanoparticles. According to the reported results for band gap energy and facts, it is clearly evidenced that the trimetallic silica nanohybrid incorporated CA-mat should be the best material that generates ROS and exhibits the best antimicrobial activity. However, all

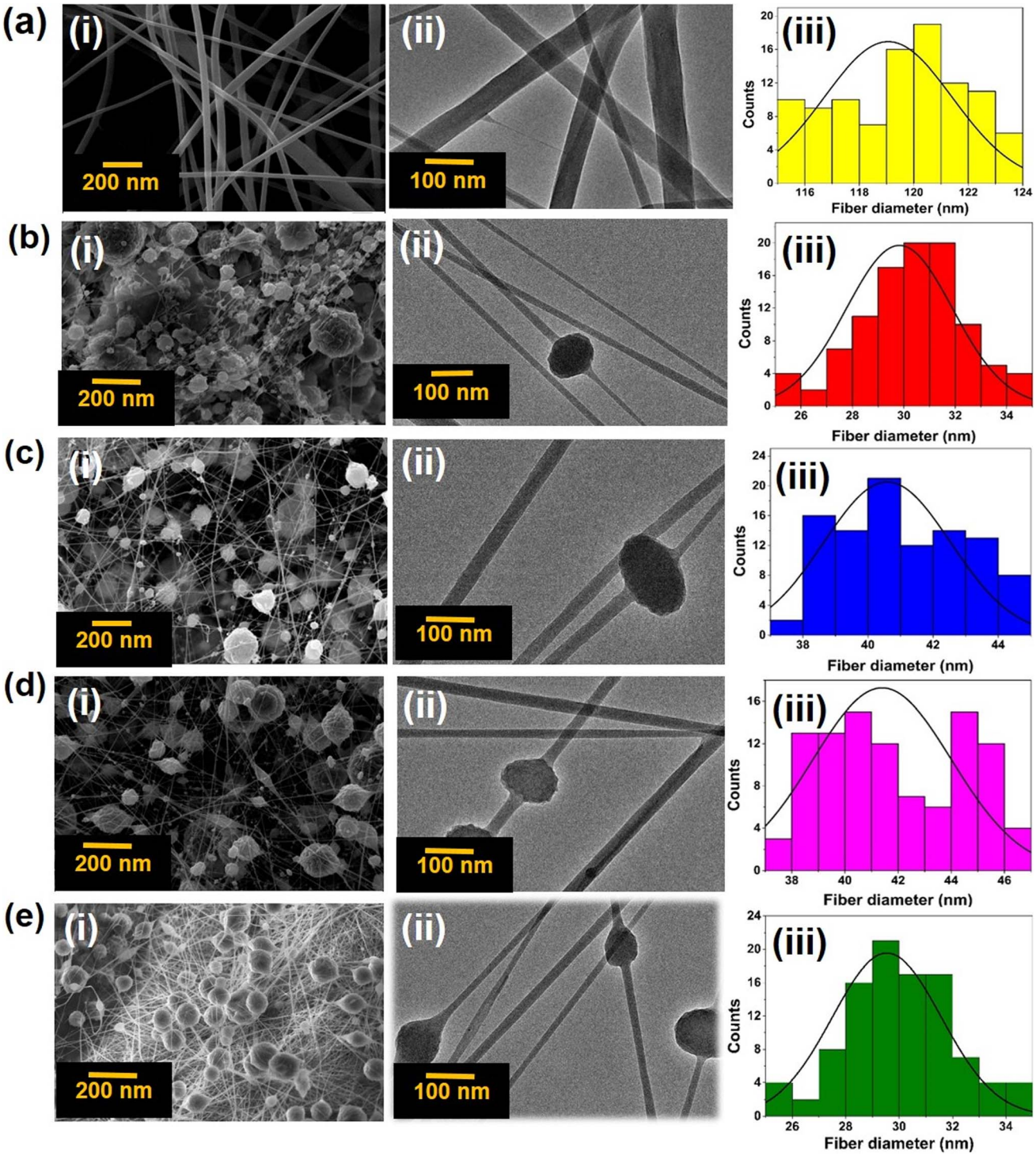

Fig. 3 (a) CA-mat, (b) Ag-Si-CA-mat, (c) Cu-Si-CA-mat, (d) Co-Si-CA-mat, (e) Ag-Si + Cu-Si + Co-Si-CA-mat; (i) the SEM imaging, (ii) the TEM imaging and (iii) distribution of the fiber diameter.

the calculated band gap energies were below 3.00 eV, therefore it is confirmed that these fabricated CA-mats possess a visible light active ROS generation that governs the self-sterilizing ability of these nanofiber mats.[86]

After confirming the lowest band gap energy by the fabricated trimetallic silica nanohybrid incorporated nanofiber mat which holds an area of 121 cm^2 (11 × 11 cm), five samples (each 1 cm × 1 cm) were taken at five different places. Then these samples were evaluated for their band gap energy. Then the evaluated band gap energies were compared to confirm the homogeneity of the band gap energy at any place on the nanofiber mat. The graphs of $(F(R)h\nu)^2$ *versus* $h\nu$ for metal doped

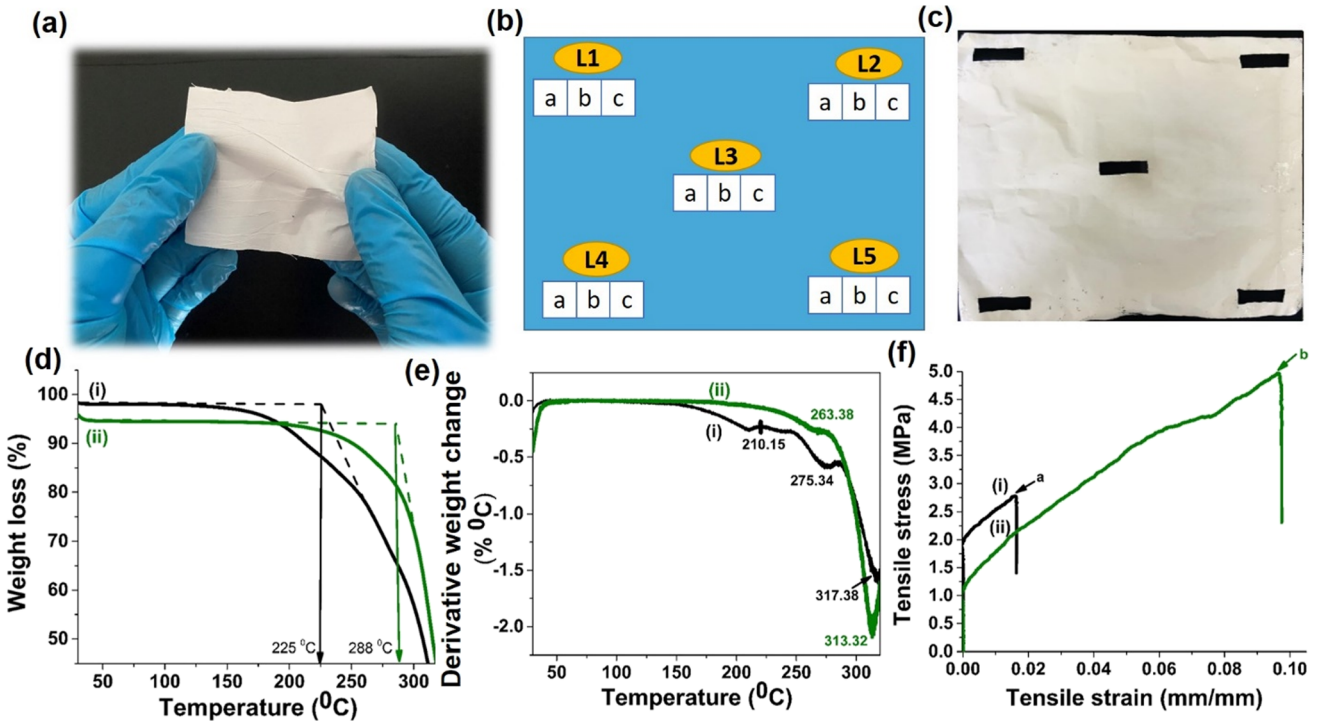

Fig. 4 (a) A digital photograph of a 50% w/w Ag-Si + Cu-Si + Co-Si-CA-mat; (b) and (c) the points where the samples were obtained to analyze band gap energies and metal composition *via* AAS analysis to confirm the homogenous distribution of each metal throughout the nanofiber mat; (d) TGA curve; (e) DTGA curve and (f) Tensile strength of (i) CA-mat, (ii) 50% w/w Ag-Si + Cu-Si + Co-Si-CA-mat.

Table 2 Reported band gap energies of metallic silica nanohybrid incorporated cellulose acetate mat

Nanofiber mat	Band gap energy (eV)
50% w/w Ag-Si-CA-mat	2.88
50% w/w Ag-Si-CA-mat	2.89
50% w/w Co-Si-CA-mat	2.92
50% w/w Ag-Si + Cu-Si + Co-Si-CA-mat	2.84

Table 3 Reported band gap energies at different places of 50% w/w trimetallic silica nanohybrid incorporated cellulose acetate mat[a]

Place of the nanofiber mat	Band gap energy (eV)
L1	2.84
L2	2.83
L3	2.84
L4	2.84
L5	2.84

[a] Considering the aforementioned results, it is clearly evidenced the homogeneity of the band gap energy at different places of the trimetallic silica nanohybrid incorporated CA-mat. It was assumed that these selected places represent the whole CA-mat.

SiNP and trimetallic silica nanohybrid incorporated cellulose acetate mat were depicted in ESI data† file 02. Table 3 shows the respective band gap energy of each point (Fig. 4(b)).

In order to examine the quantities of metals that are incorporated into the electrospun membranes (Fig. 4(a)), the selected 1 cm^2 areas a, b, and c from each location (L1, L2, L3, L4 and L5) (Fig. 4(b)) of the fabricated CA-mats were manually digested by an appropriate combination of acids (HCl and conc. HNO_3 in a ratio of 3 : 1) following their morphological and structural characterization. It provided evidence that the electrospun cellulose acetate mat's integrated metals, which are doped in silica nanohybrids, were evenly dispersed throughout. The total amount of metals in each sample per cm^2 area was then assessed using AAS analysis. According to the AAS results, Table 4 displays the mean value of the mass of each metal content at each position.

The mean values of each metal content at each point in the fabricated CA-mats were statistically analyzed in order to confirm the homogenous distribution of each metal throughout the fabricated nanofiber mat. A one-way ANOVA test was performed at the significance level of (P) 0.05. Table 5 below shows the p values of the ANOVA test. These p values confirmed that there is no significant difference between the mean values of the composition of each metal throughout the fabricated nanofiber mats, which means the distribution of each metal throughout the nanofiber mats is homogenous. After the confirmation of the homogenous distribution of each metal, the fabricated nanofiber mats were subjected to radical scavenging assays and antimicrobial assays.

The thermal stability of natural fibers plays a pivotal role in acting as a reinforcing agent, particularly considering the processing temperatures they encounter. The thermal decomposition behavior of the cellulose acetate mat and trimetallic silica nanohybrid incorporated cellulose acetate mat were

Table 4 The mean value of the mass of each metal content per cm^2 area at each point in the fabricated CA-mats

	Average mass of each metal in CA-mats (mg cm^{-2})					
	50% w/w Ag-Si-CA-mat	50% w/w Cu-Si-CA-mat	50% w/w Co-Si-CA-mat	50% w/w Ag-Si + Cu-Si + Co-Si-CA-mat		
The point of the electrospun nanofiber mat as depicted in Fig. 4	Ag	Cu	Co	Ag	Cu	Co
L1	1.75 ± 0.01	1.72 ± 0.06	1.58 ± 0.01	0.59 ± 0.01	0.58 ± 0.01	0.55 ± 0.01
L2	1.75 ± 0.06	1.73 ± 0.02	1.57 ± 0.01	0.60 ± 0.01	0.59 ± 0.02	0.55 ± 0.01
L3	1.76 ± 0.06	1.74 ± 0.06	1.59 ± 0.06	0.60 ± 0.01	0.57 ± 0.01	0.55 ± 0.02
L4	1.75 ± 0.01	1.76 ± 0.01	1.58 ± 0.01	0.61 ± 0.01	0.58 ± 0.02	0.54 ± 0.01
L5	1.74 ± 0.06	1.75 ± 0.06	1.57 ± 0.06	0.60 ± 0.02	0.58 ± 0.01	0.57 ± 0.02

Table 5 *p* values for each comparison of mean values of metal composition in nanofiber mats by one-way ANOVA test

Type of the nanofiber mat	Type of the metal	*p* value
50% w/w Ag-Si-CA-mat	Ag	0.62
50% w/w Cu-Si-CA-mat	Cu	0.13
50% w/w Co-Si-CA-mat	Co	0.58
50% w/w Ag-Si + Cu-Si + Co-Si-CA-mat	Ag	0.88
	Cu	0.92
	Co	0.71

investigated using TGA and the first derivative curve (DTGA), as shown in Fig. 4(d) and (e) respectively. According to the literature, the TGA curve of the pure cellulose acetate exhibited two main degradation areas, first one is approximately 10–15% degradation loss between the temperature ranges of 100–300 °C. The second part of the decomposition takes place at the temperature range of 300–385 °C which is approximately 80% of its initial weight. According to the DTGA curves of the electrospun mats which are shown in Fig. 4(e), the thermal decomposition can be observed well. The onset degradation temperature was reported as 210.15 °C in pure CA mats whereas the trimetallic silica nanohybrids incorporated CA mats were reported as 263.38 °C and it liberated CO and CO_2 at the temperature above 275 °C.[65,66]

The electrospun trimetallic silica nanohybrids incorporated CA mat is thermally stable up to 288 °C whereas the CA mat is thermally stable up to 225 °C. Considering the DTGA data, it can be revealed that the onset degradation temperature has increased in trimetallic silica nanohybrids incorporated CA mat when compared with pure CA mat (210.15 to 263.38 °C). Finally, it can be concluded that the incorporation of silica nanohybrids to the CA mat results in an enhancement of the thermal stability of the product, which is advantageous in employing this nanohybrids incorporated CA mat as a practical application in high temperatures as well.[65,66]

Table 6 The tensile strengths and tensile strains of electrospun CA mats

Electrospun mat	Tensile strength (MPa)	Tensile strain (%)
CA-mat	2.78 ± 1.04	1.59 ± 0.91
50% w/w Ag-Si + Cu-Si + Co-Si-CA-mat	4.99 ± 089	9.64 ± 3.73

Then the tensile strength of the CA-mat and 50% w/w Ag-Si + Cu-Si + Co-Si-CA-mat was measured to further analyze the mechanical properties of the electrospun mats. Table 6 shows the evaluated tensile strengths of each mat.

According to the reported results, it was revealed that there is a significant improvement in tensile strength and tensile strain of the trimetallic silica nanohybrid incorporated CA mat when compared with the CA mat. Much research have proved that the tensile strength of electrospun CA fibers lies between 1–2.5 MPa.[67,68] Here, it has proved that the incorporation of metallic silica nanohybrids into the CA mat strengthens the fiber mat while giving a promise to be used this fabricated trimetallic silica nanohybrid incorporated CA mat as a mechanically stable membrane in biomedical applications.

The mechanical properties of cellulose acetate-based electrospun membranes were well studied by many researchers. It was proven for its ideal mechanochemical stability to employ for various purposes. Borges *et al.* have proven its recovery and reutilization *via* straightforward mechanochemical treatment in a solid basic media to perhaps hydrolyze acetate moieties and lower particle size at the same time.[86] Moreover, Shukla *et al.* have studied a range of mechanical properties of cellulose acetate membranes that accelerate the employment of cellulose acetate-based polymer membranes in various applications.[87]

Afterwards, ICP-MS analysis was performed in order to analyze the leach out of metals; Ag, Cu, and Co from the trimetallic silica nanohybrid incorporated CA mat in culture media. There was not any detection of Ag, Cu, or Co at the detection level of 1 ppb in trimetallic silica nanohybrid incorporated CA mat incorporated culture media even after 24 hours. Hence, it revealed that there is not a leach out of metals from the trimetallic silica nanohybrid incorporated CA mat. Therefore, it is advantageous as a biomedical application because leaching out of metal nanoparticles to the medium causes some nanotoxicity and deposition in biological tissues.[44,45,88,89] Therefore the fabricated trimetallic silica nanohybrid incorporated CA mat is safe to use in personal protective devices as a functional antimicrobial layer. As a result, it can be predicted

that the generation of ROS can be the reason behind the antimicrobial activity of silica nanohybrids incorporated in CA mats. DPPH assay was performed to confirm it.

3.3 DPPH assay for evaluating the radical scavenging activity of the fabricated metal nanohybrid incorporated nanofiber mats

The DPPH radical scavenging assay was used to evaluate the rationale for the antimicrobial synergy of multimetallic silica nanohybrid-incorporated nanofiber mats *vs.* monometallic silica nanohybrid-incorporated nanofiber mats. A variety of pathways contribute to metal nanoparticles' antimicrobial activity.[88,89] Reactive oxygen species (ROS) production is an important component of radical scavenging activity. Various inorganic metal nanoparticles used as antimicrobial agents produce various ROS, hence the antibacterial mechanisms may differ. Here, we assessed and compared the radical scavenging activity of each monometallic silica nanohybrid incorporated nanofiber mat, multimetallic silica nanohybrid incorporated nanofiber mat, and CA-mat as shown in Fig. 5. The trimetallic silica nanohybrid incorporated nanofiber mat has the highest radical scavenging activity (91.77 ± 0.88%). When considering the monometallic silica nanohybrids incorporated nanofiber mats, Ag-Si-CA-mat shows the highest radical scavenging activity (80.52 ± 0.67%), whereas Co-Si-CA-mat shows the lowest radical scavenging activity (56.74 ± 1.23%). Cu-Si-CA-mat also shows a comparable radical scavenging activity (71.35 ± 1.85%) to Ag-Si-CA-mat.

Examining the results of the DPPH assay in greater context reveals a connection to the well-known semiconductor-based photocatalysis theorem. This theorem's mechanism has the potential to be employed to explain precisely why nanohybrids can scavenge free radicals in the presence of DPPH in a methanolic solution. It consists of the valence band holes (h^+), which are generated upon bandgap photoexcitation, oxidized H_2O into the OH ions, and/or the terminal OH– groups existing on the outermost layer of nanohybrids.[45] Molecular oxygen in the surrounding atmosphere scavenged the generated electrons (e^-) in the conduction band at the same time, initiating a chain reaction that ultimately produced additional hydroxyl radicals.[58] The hydroxyl surface groups clung to the holes, producing OH radicals that accelerated the degradation of organic dyes like DPPH. The unstable methanolic DPPH solution, which is purple in color, changed into a yellow color stable DPPH protonated version throughout the DPPH free-radical scavenging procedure, in agreement with the mechanism described by Kedare *et al.* By transferring electrons from the O atoms to the odd electrons in the N atoms, DPPH is changed into DPPH free radicals, which produce stable DPPH molecules.[90] Nonetheless, the DPPH assay offered convincing proof to support the antimicrobial synergy of metallic silica nanohybrids incorporating nanofiber mats.

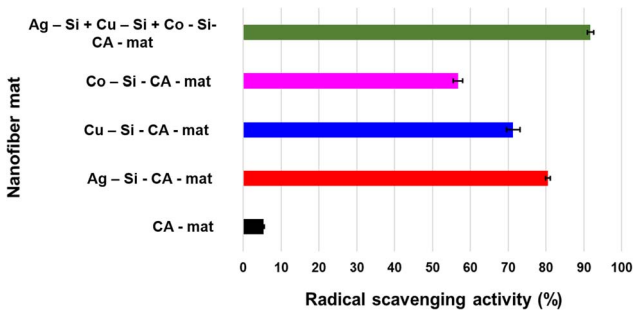

Fig. 5 Radical scavenging activity of fabricated metal nanohybrid incorporated CA-mats.

3.4 Disc diffusion assay for ATCC strains and clinical isolates of selected microbial strains to evaluate the synergistic antimicrobial activity of metal nanohybrid incorporated CA-mats

After the IC-PMS analysis, a disc diffusion experiment was utilized to determine the synergistic antimicrobial activity of multimetallic silica nanohybrids incorporating nanofiber matting. This disc diffusion assay shows how well an antibiotic therapy works against specific microbes. It is predicated on the inhibitory zones surrounding the discs that were placed on the surface of the agar plates. Here, we initially employed the disc diffusion assay to test selected ATCC strains of microorganisms, including bacteria and fungi. The inhibition zones of the several nanofiber mats against the ATCC stains of test microbes are displayed in ESI data† file 03 (figure and a table), which lists the inhibition zone values that different nanofiber mats have displayed.

A statistical analysis was then performed by two sample *t* tests to confirm that there is a significant difference between the zones of inhibitions of monometallic silica nanohybrids incorporated nanofiber mats (Ag-CA-mat, Cu-Si-CA-mat, and Co-Si-CA-mat) and the trimetallic silica nanohybrid incorporated CA-mat (Ag-Si + Cu-Si + Co-Si-CA-mat) at the significance level of 0.05. Fig. 6 shows the respective zones of inhibition and evaluates significant differences. ESI data† file 04 shows the *p* values of the statistical tests. The reported *p* values are lower than the employed significance level of 0.05. Hence, it can be interpreted that there is a significant difference between the mean values of inhibition zones of each monometallic silica nanohybrids incorporated nanofiber mats and trimetallic silica nanohybrid incorporated CA-mat (Ag-Si + Cu-Si + Co-Si-CA-mat) at the significance level of 0.05, when equal variance is assumed.[45]

The assays for clinical isolates of ATCC strains and quality control strains of the examined microbes were conducted to proceed with the disc diffusion assay. To determine the antimicrobial synergy of metallic silica nanohybrids incorporated CA-mats, antimicrobial experiments using solely ATCC strains are sufficient. To gain a thorough understanding of the antimicrobial synergy of the fabricated metallic silica nanohybrids incorporated CA-mats, we thus conducted a disc-diffusion evaluation using clinical isolates of previously evaluated ATCC strains and quality control strains. The inhibitory zones of several nanofiber mats *versus* clinical isolates of previously evaluated ATCC strains of test microorganisms are displayed in ESI data† file 05 as a figure. It has also tabulated the inhibition

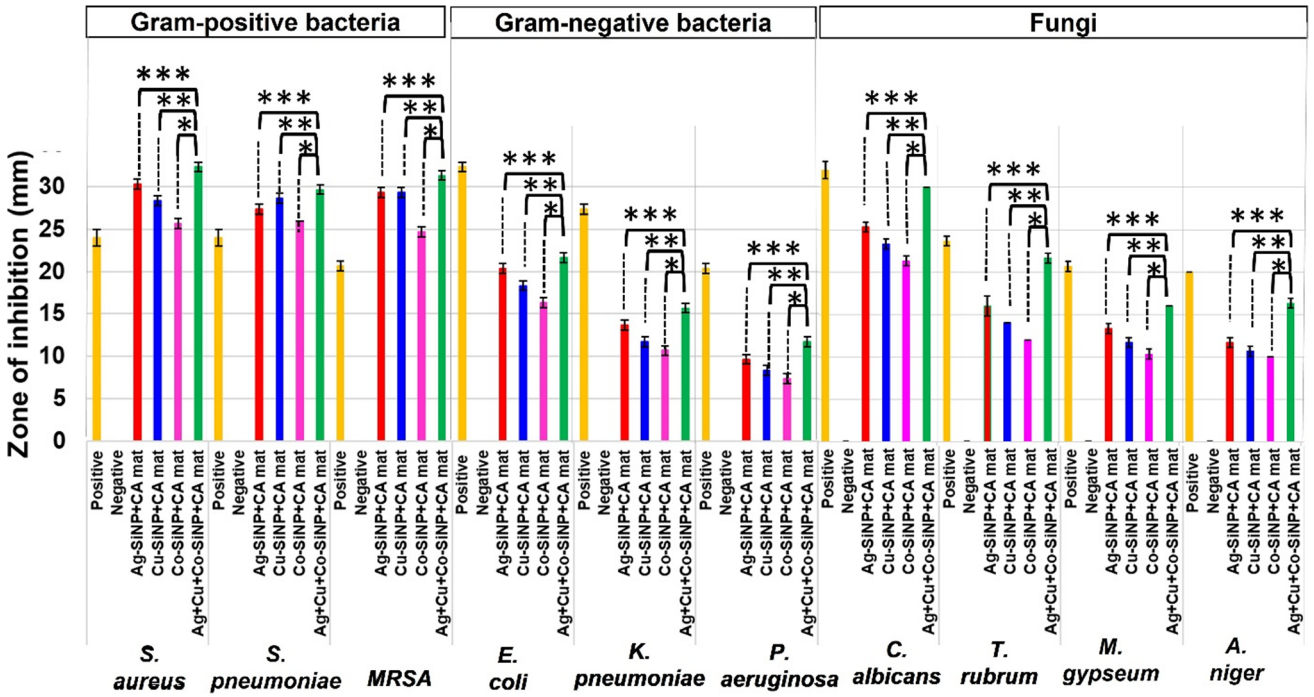

Fig. 6 The inhibition zone values of different metallic silica nanohybrids incorporated nanofiber mats against ATCC cultures of microbes; the significant difference between, (***) Ag-Si-CA-mat and Ag-Si + Cu-Si + Co-Si-CA-mat, (**) Cu-Si-CA-mat and Ag-Si + Cu-Si + Co-Si-CA-mat and (*) Co-Si-CA-mat and Ag-Si + Cu-Si + Co-Si-CA-mat.

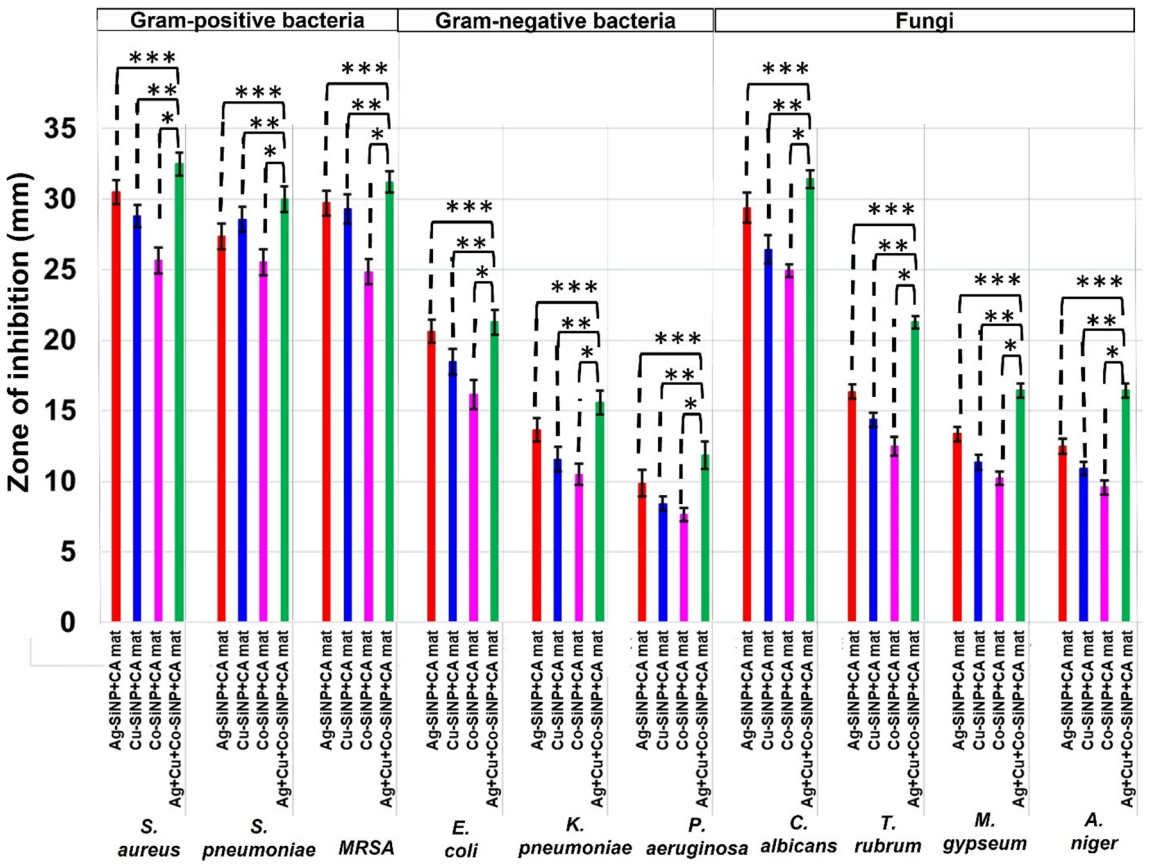

Fig. 7 The inhibition zone values of different metallic silica nanohybrids incorporated nanofiber mats against clinical isolates of selected microbes as a graphical interpretation; The significant difference between, (***) Ag-Si-CA-mat and Ag-Si + Cu-Si + Co-Si-CA-mat, (**) Cu-Si-CA-mat and Ag-Si + Cu-Si + Co-Si-CA-mat and (*) Co-Si-CA-mat and Ag-Si + Cu-Si + Co-Si-CA-mat.

zone values that different nanofiber mats (ESI data† file 05-tables). For each microbial strain, we used five clinical isolates ($N = 5$) for each selected type of microbial strain in this instance.[45]

It is evident that the findings of the analysis of the zones of inhibition of fabricated nanofiber mats over clinical isolates correlate well with the zones of inhibition towards ATCC strains. Fig. 7 shows the mean values for zones of inhibition displayed by nanofiber mats towards all five clinical strains for each microbe including triplicates of them ($N = 15$ for each type of fungi), of formerly evaluated ATCC strains. A statistical analysis was performed in this instance also by two-sample *t* test to confirm that there is a significant difference between the zones of inhibitions of monometallic silica nanohybrids incorporated nanofiber mats (Ag-Si-CA-mat, Cu-Si-CA-mat, and Co-Si-CA-mat) and the trimetallic silica nanohybrid incorporated CA-mat (Ag-Si + Cu-Si + Co-Si-CA-mat) at the significance level of 0.05. ESI data† file 06 shows the *p* values of the statistical tests. The reported *p*-values are lower than the employed significance level of 0.05.[45]

Hence, it can be interpreted that there is a significant difference between the mean values of inhibition zones of each monometallic silica nanohybrids incorporated nanofiber mats and trimetallic silica nanohybrid incorporated CA-mat (Ag-Si + Cu-Si + Co-Si-CA-mat) at the significance level of 0.05, when equal variance is assumed. These reported results are also in good agreement with the results of the two-sample *t*-test that was performed for ATCC strains of these organisms. Hence, it is confirmed that the fabricated Ag-Si + Cu-Si + Co-Si-CA-mat exhibits the best antimicrobial synergy against both ATCC strains and clinical isolates of the tested microorganisms.

Considering the results, the highest antimicrobial activity of monometallic silica nanohybrids incorporated CA-mat was shown by Ag-Si-CA-mat. Co-Si-CA-mat exhibited the lowest zone of inhibition against all the test strains of microbes. The trimetallic silica nanohybrid incorporated CA-mat showed the highest zone of inhibition against all the test microorganisms. Among Gram-positive bacteria, *Staphylococcus aureus* and *Streptococcus pneumoniae* possess the highest values for zones of inhibition. MRSA has lower values for the zone of inhibition; this may be due to its widely known resistant mechanisms.[90,91] However, the fabricated nanofiber mats are effective against methicillin-resistant *Staphylococcus aureus.* When analyzing the zones of inhibition of Gram-negative bacteria, *E. coli* possesses the greatest values, while *Pseudomonas aeruginosa* and *Klebsiella pneumoniae* possess lower values. These two-gram negative bacteria are considered that show a high degree of antibiotic resistance. *Klebsiella pneumoniae* and *Pseudomonas aeruginosa* are also known as "superbugs", which are also referred to as microbes that show resistance to at least three antimicrobial agents.[92–94] However, the fabricated nanofiber mats in this study have also exhibited antibacterial activity against these bacteria.

Regarding the antifungal activity of the fabricated CA-mats, they are also in good agreement with the results for bacteria. The highest antifungal activity of monometallic silica nanohybrids incorporated CA-mat was shown by Ag-Si-CA-mat. Co-Si-CA-mat exhibited the lowest zone of inhibition against all the test strains of fungi. The trimetallic silica nanohybrid incorporated CA-mat showed the highest zone of inhibition against all the tested fungi. When comparing the zones of inhibition, it is evident that *C. albicans* show higher zones of inhibition than the filamentous fungi (*T. rubrum*, *M. gypseum, A. niger*). This is an important finding as some skin rashes are mainly due to this yeast, *Candida albicans*. Candida is a commensal that resides on our skin and causes opportunistic infections such as Candida skin infection and vaginal Candidiasis. Filamentous fungi are a type of fungi that have a well-organized cell structure other than yeast type of fungi. This may be the reason for the differences that were observed in the respective zones of inhibition.[61–63]

Considering the antibacterial activity and the antifungal activity, it can be clearly observed that the trimetallic silica nanohybrid incorporated CA-mat exhibits greater antibacterial activity than antifungal activity except for resistant strains. Fungal cells are eukaryotic cells which means they have a well-organized cellular structure with a nucleus when compared with bacterial cells because bacteria are prokaryotic cells. This may be caused for the observations. However, according to the reported results, this multimetallic silica nanohybrid incorporated CA-mat will be a potential new hope for the development of emerging PPE and personal hygiene products against a broad spectrum of microbes including Gram-positive and Gram-negative bacteria, yeast-type fungi, and filamentous fungi.[45,62,63]

3.5 SEM imaging of microbial cultures when exposing to the fabricated multimetallic silica nanohybrid incorporated CA-mat

As shown in the Fig. 8, finally a SEM analysis was carried out for all the strains of tested microbes of *Staphylococcus aureus*, *Streptococcus pneumoniae*, MRSA, *Escherichia coli*, *Klebsiella pneumoniae*, *Pseudomonas aeruginosa*, *Candida albicans*, *Trichophyton rubrum*, *Microsporum gypseum*, and *Aspergillus niger* in order to investigate the structural deformations of these microbial cells when introducing to the multimetallic silica nanohybrid incorporated CA-mat that has already confirmed as the antimicrobial nanofiber mat which exhibits the best antimicrobial activity.

According to the observed results, it is clearly visible that the trimetallic silica nanohybrid incorporated CA-mat possesses a significant antimicrobial potential against all the tested bacteria and fungi. When observing the untreated samples, there is a massive amount of microbial cells over the trimetallic silica nanohybrid incorporated CA-mat. In some images of untreated samples, the surface of the CA-mat has been covered by microorganisms causing it unable to observe nanofibers in the mat. The amount of microbial cells in the treated samples has been drastically decreased due to the antimicrobial mechanisms of the trimetallic silica nanohybrids. There are some destroyed particles of microbial cells can be seen in these images of treated samples. This SEM imaging further provides clear evidence for the antimicrobial ability of the trimetallic silica nanohybrids incorporated CA-mat.[45]

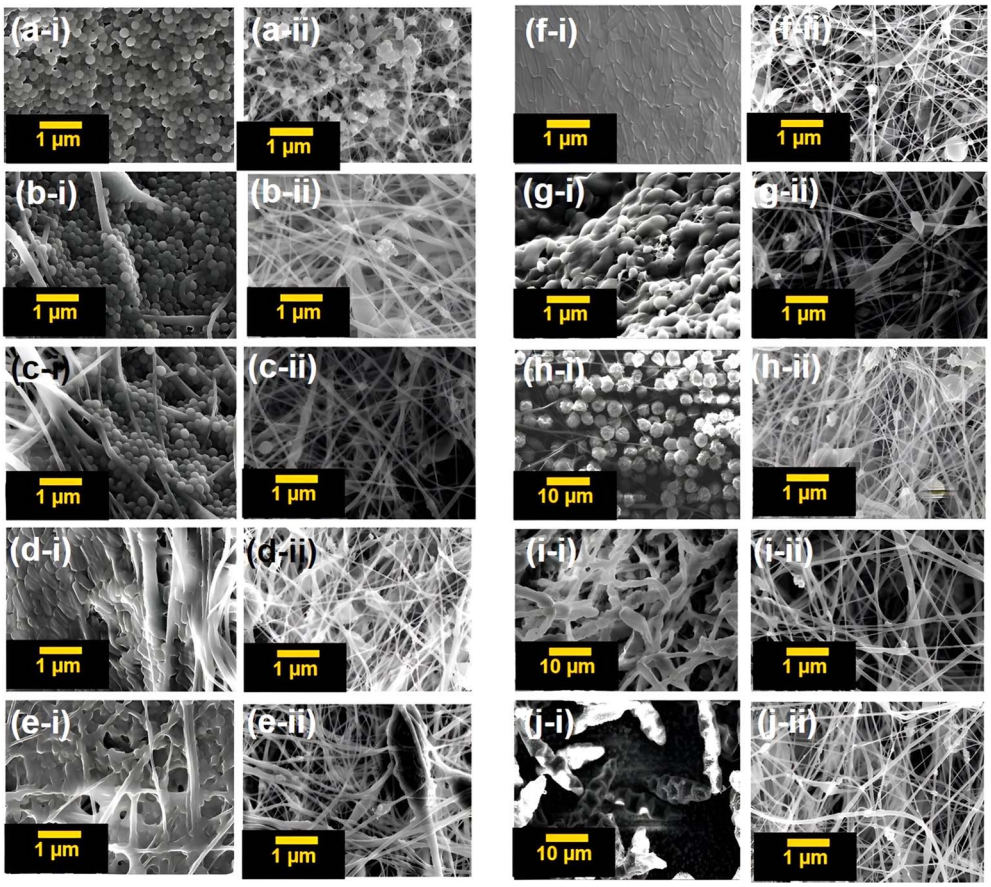

Fig. 8 (a-i) Untreated *Staphylococcus aureus*, (a-ii) treated *Staphylococcus aureus*, (b-i) untreated *Streptococcus pneumonia*, (b-ii) treated *Streptococcus pneumonia*, (c-i) untreated MRSA, (c-ii) treated MRSA, (d-i) untreated *Escherichia coli*, (d-ii) treated *Escherichia coli*, (e-i) untreated *Klebsiella pneumonia*, (e-ii) treated *Klebsiella pneumonia*. (f-i) Untreated *Pseudomonas aeruginosa*, (f-ii) treated *Pseudomonas aeruginosa*, (g-i) untreated *Candida albicans*, (g-ii) treated *Candida albicans*, (h-i) untreated *Aspergillus niger*, (h-ii) treated *Aspergillus niger*, (i-i) untreated *Microsporum gypseum*, (i-ii) treated *Microsporum gypseum*, (j-i) untreated *Trichophyton rubrum* and (j-ii) treated *Trichophyton rubrum*.

3.6 Electrospinning of the CA polymer solution including multimetallic silica nanohybrids on a diaper surface; as a practical application

Based on the previous results described, the multimetallic silica nanohybrid incorporated into the CA-mat was well-proven for its synergistic best antimicrobial activity over monometallic silica nanohybrids incorporated into the CA-mat. Therefore, we have electrospun the respective polymer solution with multimetallic silica nanohybrids on the surface of a commercially available diaper as proof of the practical application of this nanofiber mat. For this purpose, a polymer solution of cellulose acetate (10% w/v) in acetone: DMF mixture (2 : 1) was incorporated with trimetallic silica nanohybrids (50% w/w). The mixture was stirred for 2 hours and sonicated for 4 hours. Then it was electrospun on the surface of the commercially available diaper. ESI data† file 07 shows the electrospinning process and the resulting surface coating of the diaper. Fig. 9 shows the SEM images of the resulting surface coating of the diaper. The SEM analysis of the resulting nanofiber mat on the surface of the diaper was performed by freeze fracturing[95] the resulting

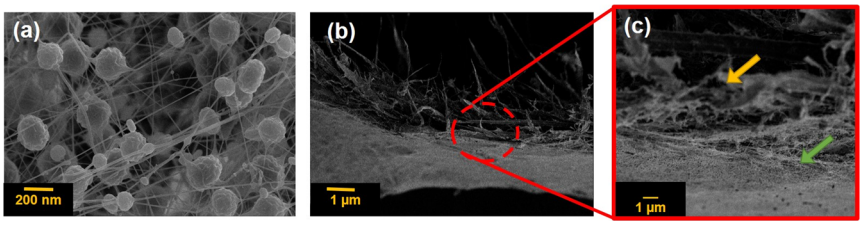

Fig. 9 (a) SEM image of the 50% w/w multimetallic silica nanohybrid incorporated CA-mat on the diaper surface, (b) and (c) SEM image of a cross section of 50% w/w multimetallic silica nanohybrid incorporated CA-mat on the diaper surface.

composite material in order to investigate the morphological characteristics of the material.

The SEM image of the surface clearly depicts the spherical silica nanohybrids and the thin nanofibers on the diaper surface. The SEM image of the cross section depicts the fibers of the CA nanofiber membrane and the fibers of the diaper material. In Fig. 9(c), the yellow arrows showed the fibers of the diaper material, and the green arrows showed the nanofibers of the CA-mat. In the CA-mat, there can be observed the incorporated silica nanohybrids as tiny black dots.

3.7 Antimicrobial assay for multimetallic silica nanohybrid incorporated CA-mat on the diaper surface

The antimicrobial assay for the multimetallic silica nanohybrid incorporated CA-mat on the diaper surface was carried out by disc diffusion assay according to the method described in Section 3.4. The discs of the electrospun membrane (diameter = 6 mm) were soaked in artificial urine (40 mL) for different time durations; 2 h, 4 h, 8 h, 16 h, 24 h-upside, and 24 h downside. Artificial urine was made according to the method described by Shmaefsky *et al.*[95]

ATCC strains of three Gram-positive organisms; *Staphylococcus aureus,* MRSA, and *Streptococcus pneumoniae*, and three Gram-negative bacteria *Escherichia coli, Klebsiella pneumoniae*, and *Pseudomonas aureginosa* were used. The prepared media and tips of the micropipette were sterilized in an autoclave at 121 °C for 1 hour. Other glassware was sterilized in an oven at 100 °C for 1 hour. The disks of polymer membranes were kept in contact with UV light for 30 minutes for sterilization. A commercial antimicrobial agent (Erythromycin 10 μg and Gentamycin 15 μg) is used as the positive control. A disc from the commercially available diaper was used as the negative control. Disks are placed on the surface of the solidified agar by using sterile forceps. The plates are then immediately inverted and incubated at 37 °C for 24 hours. Then the zones of inhibition are observed. Table 7 shows the inhibition zones of the respective discs of electrospun nanofiber mats at different time intervals. All the studies were triplicated. Fig. 10 shows the inhibition zones of the respective disc.

Table 7 The inhibition zones of the respective discs of electrospun nanofiber mats at different time intervals

Metallic silica nanohybrids incorporated electrospun membranes on the diaper surface	Zone of inhibition (mm)					
	S. aureus	*S. pneumoniae*	MRSA	*E.coli*	*K. pneuminiae*	*S. aureus*
Positive control	35.00 ± 1.00	30.67 ± 0.58	35.00 ± 1.00	32.33 ± 0.58	25.33 ± 0.58	25.00 ± 1.00
Negative control	—	—	—	—	—	—
2 h	32.33 ± 0.58	29.67 ± 0.58	32.33 ± 0.58	21.67 ± 0.58	15.67 ± 0.58	11.33 ± 0.58
4 h	32.33 ± 0.58	30.33 ± 0.58	32.33 ± 0.58	21.33 ± 0.58	15.33 ± 0.58	11.67 ± 0.58
8 h	32.67 ± 0.58	29.67 ± 0.58	32.33 ± 0.58	21.67 ± 0.58	15.33 ± 0.58	11.33 ± 0.58
16 h	32.00 ± 1.00	29.33 ± 0.58	32.33 ± 0.58	21.67 ± 0.58	15.67 ± 0.58	11.67 ± 0.58
24h (U)	31.67 ± 0.58	29.67 ± 0.58	32.33 ± 0.58	21.67 ± 0.58	15.33 ± 0.58	11.67 ± 0.58
24 h (D)	31.67 ± 0.58	29.33 ± 0.58	32.67 ± 0.58	21.33 ± 0.58	15.67 ± 0.58	11.67 ± 0.58

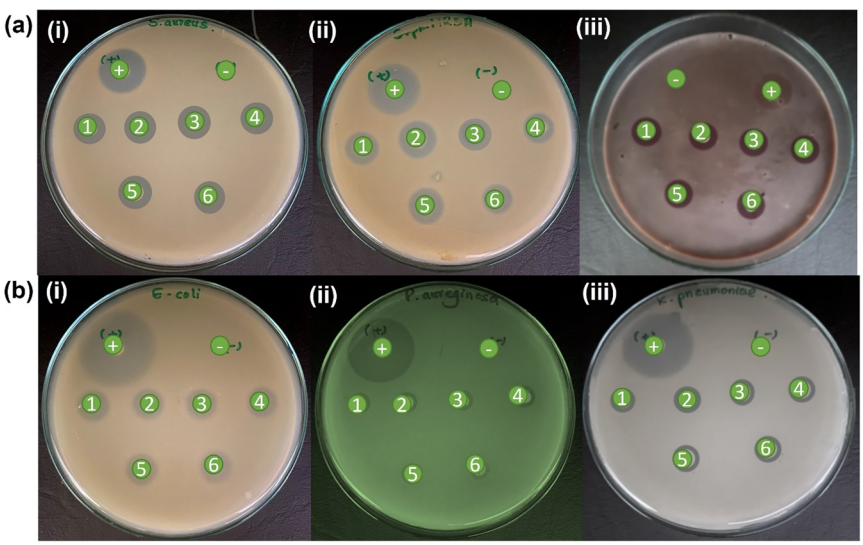

Fig. 10 Zones of inhibition of (a) Gram positive bacteria; (i) *Staphylococcus aureus*, (ii) MRSA, (iii) *Streptococcus pneumonia*; (b) Gram negative bacteria; (i) *Escherichia coli*, (ii) *Pseudomonas aeruginosa,* (iii) *Klebsiella pneumoniae*; (+) Positive control, (−) negative control, the discs of nanofiber mat on the diaper surface at; (1) 2 h, (2) 4 h, (3) 8 h, (4) 16 h, (5) 24 h – U and (6) 24 h – D.

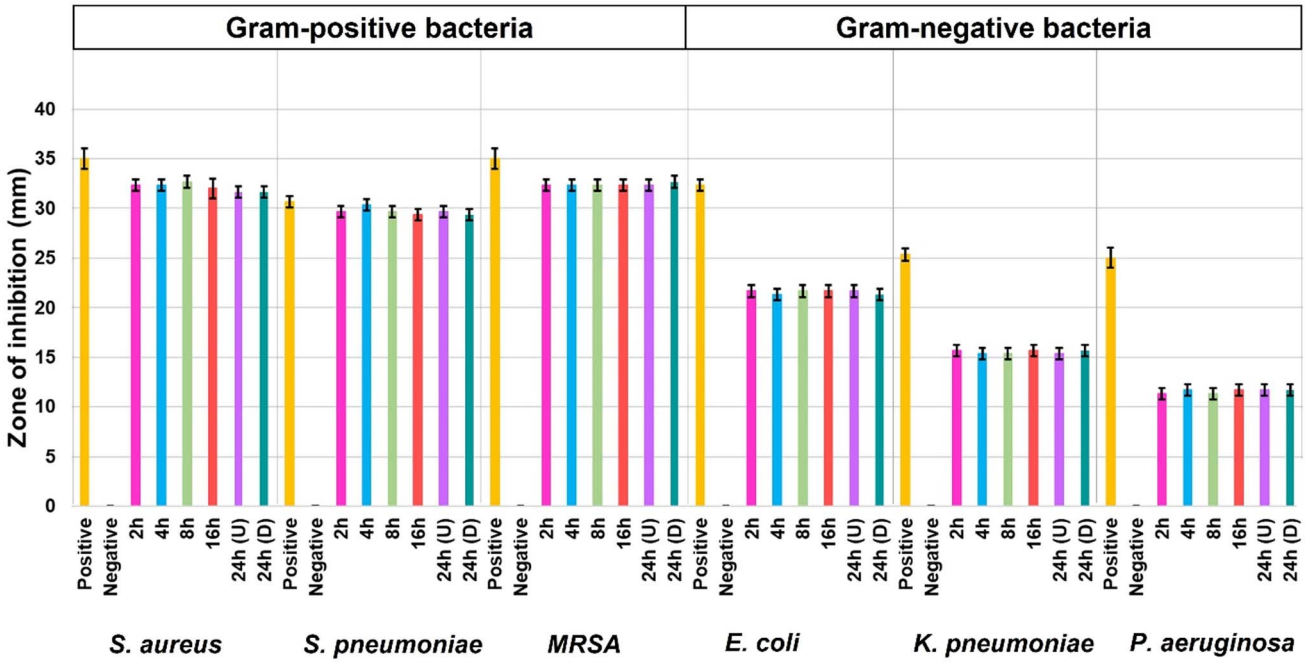

Fig. 11 The respective zones of inhibition at different time intervals against tested ATCC strains of microbes.

According to the reported results, it is evidenced that the antimicrobial activity of CA-mat on the diaper surface did not differ with time. Here we performed the experiment up to 24 hours of exposure to artificial urine. At 24 hours, there were two discs were employed labeled as 24 h – upside and 24 h – downside. It investigated the antimicrobial activity of both sides of metallic silica nanohybrid incorporated CA-mat on the diaper surface. The advantage here is this material can be employed as an inner layer in diapers, PPE, or other personal hygiene products without contacting the skin while the antimicrobial activity remains constant. Fig. 11 shows the respective zones of inhibition at different time intervals against tested ATCC strains of microbes.

Afterward, A one-way ANOVA was performed to confirm that there is no significant difference between the mean values of inhibition zones at each time interval, which means the antimicrobial activity of the multimetallic silica nanohybrid incorporated CA-mat on the diaper surface remains constant over a period of 24 h. The significance level of (P) 0.05 was employed. ESI data† file 08 shows the *p* values of the one-way ANOVA test performed. The calculated *p* values were greater than the *P* value of 0.05, which means there is no significant difference among the mean values of the inhibition zones at different time intervals (ESI data† file 08). This confirms that there is an antimicrobial activity of multimetallic silica nanohybrid incorporated CA-mat which remains constant for up to 24 hours.[45] With the proven antimicrobial results along with the well-proven mechanical and thermal properties, this trimetallic silica nanohybrid CA-mat can be developed as a self-sterilizing antimicrobial layer for broad-spectrum coverage of microbes.[96,97]

4 Conclusion

According to our results, it is evidenced that the fabricated trimetallic silica nanohybrid incorporated CA-mat possesses a promising antimicrobial potential against the tested microbes. These microbes include Gram-positive bacteria, Gram-negative bacteria, yeast-type fungi, and filamentous-type fungi. Hence, it is significant for its broad-spectrum coverage of microbes, which the conventional antimicrobial agents are incapable of. The band gap energy of 2.84 eV trimetallic silica nanohybrid incorporated CA-mat proved that it is activated under visible light. Therefore, this fabricated CA-mat can be developed as a self-sterilizing material to be employed as an antimicrobial layer in many biomedical applications. The fiber diameter of the nanofiber mat was also decreased with the incorporation of metals giving rise to high penetrability to visible light into the nanofibers. This ensures the activation of ROS generating and initiating the antimicrobial activity. Finally, it can be concluded that this trimetallic silica nanohybrid incorporated CA-mat ensures the availability, affordability, activity against a broad spectrum of microbes, cost-effectiveness, and biodegradability which act as both a physical and biological barrier for microbes.

Data availability

Data will be made available on request.

Author contributions

P. Yapa – conduct experiment, formal analysis of data and writing the manuscript. I.Munaweera – conceptualization,

funding acquisition, methodology, supervision, writing, review and editing the original draft. L. Weerasinghe – supervision, formal analysis of data, review and editing the original draft. M. Weerasekera – supervision, curation of microbiology data, review and editing the original draft. All authors have approved the final version of the manuscript.

Conflicts of interest

The authors declare that there is no conflict of interest.

Acknowledgements

Financial support for this study is acknowledged by the University of Sri Jayewardenepura, Sri Lanka under the research grant number ASP/01/RE/SCI/2022/15 and The World Academy of Science (20/102/RG/CHE/AS_1 – FR3240314134) for providing grants for the electrospinning setup. Authors acknowledge the Instrument Centre, Faculty of Applied Sciences, University of Sri Jayewardenepura for the facility provided in analysis and characterization.

References

1 S. Szabó, B. Feier, D. Capatina, M. Tertis, C. Cristea and A. Popa, An overview of healthcare associated infections and their detection methods caused by pathogen bacteria in Romania and Europe, *J. Clin. Med.*, 2022, **11**(11), 3204, DOI: **10.3390/jcm11113204**.

2 L. Turtle, M. Thorpe, T. M. Drake, M. Swets, C. Palmieri, C. D. Russell, *et al*, Outcome of COVID-19 in hospitalised immunocompromised patients: An analysis of the WHO ISARIC CCP-UK prospective cohort study, *PLoS Med.*, 2023, **20**(1), e1004086, DOI: **10.1371/journal.pmed.1004086**.

3 Commission for Hospital Hygiene and Infection Prevention (KRINKO), Infection prevention requirements for the medical care of immunosuppressed patients: recommendations of the Commission for Hospital Hygiene and Infection Prevention (KRINKO) at the Robert Koch Institute, *GMS Ger. Med. Sci.*, 2022, **17**, 7, DOI: **10.3205/DGKH000410**.

4 R. Reyes, R. Ahn, K. Thurber and T. F. Burke, Urbanization and infectious diseases: General principles, historical perspectives, and contemporary challenges, in *Challenges in Infectious Diseases*, Springer, New York, NY, 2013, pp. 123–146.

5 L. Fu, Q. Yang, Z. Liu, X. Liu and Z. Wang, Risk identification of major infectious disease epidemics based on complex network theory, *Int. J. Disaster Risk Reduct.*, 2022, **78**(103155), 103155, DOI: **10.1016/j.ijdrr.2022.103155**.

6 P. Prasher and M. Sharma, Nanotechnology-based self-sterilizing surfaces and their potential in combating COVID-19, *Nanomedicine*, 2021, **16**(14), 1183–1186, DOI: **10.2217/nnm-2021-0079**.

7 A. Behera, Self-Cleaning Materials, in *Advanced Materials*, Cham: Springer International Publishing, 2022, pp. 359–394.

8 M. Birkett, L. Dover, C. Cherian Lukose, A. Wasy Zia, M. M. Tambuwala and Á. Serrano-Aroca, Recent advances in metal-based antimicrobial coatings for high-touch surfaces, *Int. J. Mol. Sci.*, 2022, **23**(3), 1162, DOI: **10.3390/ijms23031162**.

9 B. Jalvo, M. Faraldos, A. Bahamonde and R. Rosal, Antimicrobial and antibiofilm efficacy of self-cleaning surfaces functionalized by TiO2 photocatalytic nanoparticles against Staphylococcus aureus and Pseudomonas putida, *J. Hazard. Mater.*, 2017, **340**, 160–170, DOI: **10.1016/j.jhazmat.2017.07.005**.

10 N. Karim, S. Afroj, K. Lloyd, L. C. Oaten, D. V. Andreeva, C. Carr, *et al*, Sustainable personal protective clothing for healthcare applications: A review, *ACS Nano*, 2020, **14**(10), 12313–12340, DOI: **10.1021/acsnano.0c05537**.

11 S. Alkarri, H. Bin Saad and M. Soliman, On antimicrobial polymers: Development, mechanism of action, international testing procedures, and applications, *Polymers*, 2024, **16**(6), 771, DOI: **10.3390/polym16060771**.

12 L. Borysiewicz, Prevention is better than cure, *Clin. Med.*, 2009, **9**(6), 572–583, DOI: **10.7861/clinmedicine.9-6-572**.

13 N. J. Rowan and J. G. Laffey, Challenges and solutions for addressing critical shortage of supply chain for personal and protective equipment (PPE) arising from Coronavirus disease (COVID19) pandemic – Case study from the Republic of Ireland, *Sci. Total Environ.*, 2020, **725**(138532), 138532, DOI: **10.1016/j.scitotenv.2020.138532**.

14 J. Cohen and Y. van der M. Rodgers, Contributing factors to personal protective equipment shortages during the COVID-19 pandemic, *Prev. Med.*, 2020, **141**(106263), 106263, DOI: **10.1016/j.ypmed.2020.106263**.

15 C. J. Park, R. Barakat, A. Ulanov, Z. Li, P.-C. Lin, K. Chiu, *et al*, Sanitary pads and diapers contain higher phthalate contents than those in common commercial plastic products, *Reprod. Toxicol.*, 2019, **84**, 114–121, DOI: **10.1016/j.reprotox.2019.01.005**.

16 K. Skowron, J. Bauza-Kaszewska, Z. Kraszewska, N. Wiktorczyk-Kapischke, K. Grudlewska-Buda, J. Kwiecińska-Piróg, *et al*, Human skin microbiome: Impact of intrinsic and extrinsic factors on skin Microbiota, *Microorganisms*, 2021, **9**(3), 543, DOI: **10.3390/microorganisms9030543**.

17 A. L. Byrd, Y. Belkaid and J. A. Segre, The human skin microbiome, *Nat. Rev. Microbiol.*, 2018, **16**(3), 143–155, DOI: **10.1038/nrmicro.2017.157**.

18 P. Collignon and S. McEwen, One Health—its importance in helping to better control antimicrobial resistance, *Trop. Med. Infect. Dis.*, 2019, **4**(1), 22, DOI: **10.3390/tropicalmed4010022**.

19 S. F. Shah, N. S. Punjani, S. N. Rizvi, S. S. Sheikh and R. Jan, Knowledge, attitudes, and practices regarding menstrual hygiene among girls in ghizer, Gilgit, Pakistan, *Int. J. Environ. Res. Public Health*, 2023, **20**(14), 6424, DOI: **10.3390/ijerph20146424**.

20 M. A. Salam, M. Y. Al-Amin, M. T. Salam, J. S. Pawar, N. Akhter, A. A. Rabaan, *et al*, Antimicrobial resistance: A

growing serious threat for global public health, *Healthcare*, 2023, **11**(13), 1946, DOI: 10.3390/healthcare11131946.

21 S. Kumwenda, Challenges to hygiene improvement in developing countries, in *The Relevance of Hygiene to Health in Developing Countries*, IntechOpen, 2019.

22 E. Zhang, X. Zhao, J. Hu, R. Wang, S. Fu and G. Qin, Antibacterial metals and alloys for potential biomedical implants, *Bioact. Mater.*, 2021, **6**(8), 2569–2612, DOI: 10.1016/j.bioactmat.2021.01.030.

23 X. Yang, W. Zhang, X. Qin, M. Cui, Y. Guo, T. Wang, *et al*, Recent progress on bioinspired antibacterial surfaces for biomedical application, *Biomimetics*, 2022, **7**(3), 88, DOI: 10.3390/biomimetics7030088.

24 K. L. Seneviratne, I. Munaweera, S. E. Peiris, P. Kodithuwakku, C. N. Peiris and N. Kottegoda, Visible light active silver decorated iron titanate/titanium dioxide nanohybrid for sterilization of explants grown by in vitro technique, *Adv. Mater. Technol.*, 2023, **8**(6), 2201292, DOI: 10.1002/admt.202201292.

25 I. Munaweera, A. S. Pathiraja and N. Kottegoda, Surface functionalized Mesoporous Silica Nanoparticles for enhanced removal of heavy metals: A review, *VJScience*, 2023, **1**(s1), DOI: 10.31357/vjs.v1is1.6705.

26 P. Disanayake, C. Madhusha, I. Munaweera, G. Wijesinghe, M. Weerasekera, S. Deraniyagala, *et al*, Microwave-assisted synthesis of cobalt-doped rutile/ilmenite derived from natural sands as visible-light-active photocatalytic and antimicrobial agents, *ChemistrySelect*, 2022, **7**(33), e202202598, DOI: 10.1002/slct.202202598.

27 S. Modi, G. K. Inwati, A. Gacem, S. Saquib Abullais, R. Prajapati, V. K. Yadav, *et al*, Nanostructured antibiotics and their emerging medicinal applications: An overview of nanoantibiotics, *Antibiotics*, 2022, **11**(6), 708, DOI: 10.3390/antibiotics11060708.

28 K. L. Seneviratne, I. Munaweera, S. E. Peiris, C. N. Peiris, N. Kottegoda. A method of making silver-iron titanate nanoparticles and uses thereof. *US Pat.* 20240051842A1, 2024.

29 B. Koneru, Y. Shi, I. Munaweera, M. Wight-Carter, H. Kadara, H. Yuan, *et al*, Radiotherapeutic bandage for the treatment of squamous cell carcinoma of the skin, *Nucl. Med. Biol.*, 2016, **43**(6), 333–338, DOI: 10.1016/j.nucmedbio.2016.02.010.

30 C. Madhusha, K. Rajapaksha, I. Munaweera, M. de Silva, C. Perera, G. Wijesinghe, *et al*, A novel green approach to synthesize curcuminoid-layered double hydroxide nanohybrids: Adroit biomaterials for future antimicrobial applications, *ACS Omega*, 2021, **6**(14), 9600–9608, DOI: 10.1021/acsomega.1c00151.

31 S. K. Murthy, Nanoparticles in modern medicine: state of the art and future challenges, *Int. J. Nanomed.*, 2007, **2**(2), 129–141.

32 I. Munaweera, B. Koneru, Y. Shi, A. J. Di Pasqua and K. J. Jr Balkus, Chemoradiotherapeutic wrinkled mesoporous silica nanoparticles for use in cancer therapy, *APL Mater.*, 2014, **2**(11), 113315, DOI: 10.1063/1.4899118.

33 A. Haleem, M. Javaid, R. P. Singh, S. Rab and R. Suman, Applications of nanotechnology in medical field: a brief review, *Glob. Health J.*, 2023, **7**(2), 70–77, DOI: 10.1016/j.glohj.2023.02.008.

34 L. Wang, C. Hu and L. Shao, The antimicrobial activity of nanoparticles: present situation and prospects for the future, *Int. J. Nanomed.*, 2017, **12**, 1227–1249, DOI: 10.2147/ijn.s121956.

35 S. Modi, G. K. Inwati, A. Gacem, S. Saquib Abullais, R. Prajapati, V. K. Yadav, *et al*, Nanostructured antibiotics and their emerging medicinal applications: An overview of nanoantibiotics, *Antibiotics*, 2022, **11**(6), 708, DOI: 10.3390/antibiotics11060708.

36 T. Shabatina, O. Vernaya, A. Shumilkin, A. Semenov and M. Melnikov, Nanoparticles of bioactive metals/metal oxides and their nanocomposites with antibacterial drugs for biomedical applications, *Materials*, 2022, **15**(10), 3602, DOI: 10.3390/ma15103602.

37 A. I. Ribeiro, A. M. Dias and A. Zille, Synergistic effects between metal nanoparticles and commercial antimicrobial agents: A review, *ACS Appl. Nano Mater.*, 2022, **5**(3), 3030–3064, DOI: 10.1021/acsanm.1c03891.

38 Q. Zhang, S. Yan, X. Yan and Y. Lv, Recent advances in metal-organic frameworks: Synthesis, application and toxicity, *Sci. Total Environ.*, 2023, **902**(165944), 165944, DOI: 10.1016/j.scitotenv.2023.165944.

39 K. Skłodowski, S. J. Chmielewska-Deptuła, E. Piktel, P. Wolak, T. Wollny and R. Bucki, Metallic nanosystems in the development of antimicrobial strategies with high antimicrobial activity and high biocompatibility, *Int. J. Mol. Sci.*, 2023, **24**(3), 2104, DOI: 10.3390/ijms24032104.

40 R. Narayan, U. Nayak, A. Raichur and S. Garg, Mesoporous silica nanoparticles: A comprehensive review on synthesis and recent advances, *Pharmaceutics*, 2018, **10**(3), 118, DOI: 10.3390/pharmaceutics10030118.

41 S. Kumarage, I. Munaweera and N. Kottegoda, Contemporary, multidisciplinary roles of mesoporous silica nanohybrids/nanocomposites, *ChemistrySelect*, 2022, **7**(21), e202200574, DOI: 10.1002/slct.202200574.

42 V. S. Reddy, Y. Tian, C. Zhang, Z. Ye, K. Roy, A. Chinnappan, *et al*, A review on electrospun nanofibers based advanced applications: From health care to energy devices, *Polymers*, 2021, **13**(21), 3746, DOI: 10.3390/polym13213746.

43 S. Kumarage, I. Munaweera and N. Kottegoda, A comprehensive review on electrospun nanohybrid membranes for wastewater treatment, *Beilstein J. Nanotechnol.*, 2022, **13**, 137–159, DOI: 10.3762/bjnano.13.10.

44 P. Yapa, I. Munaweera, M. M. Weerasekera, L. Weerasinghe and C. Sandaruwan, Potential antifungal applications of heterometallic silica nanohybrids: A synergistic activity, *Biomater. Adv.*, 2024, **162**(213930), 213930, DOI: 10.1016/j.bioadv.2024.213930.

45 P. N. Yapa, I. Munaweera, C. Sandaruwan, L. Weerasinghe and M. M. Weerasekera, Metal doped silica nanohybrids with extensive bacterial coverage for antibacterial applications exhibit synergistic activity, *Biomater. Adv.*,

2024, **157**(213753), 213753, DOI: **10.1016/j.bioadv.2023.213753**.

46 A. M. Abdelgawad, S. M. Hudson and O. J. Rojas, Antimicrobial wound dressing nanofiber mats from multicomponent (chitosan/silver-NPs/polyvinyl alcohol) systems, *Carbohydr. Polym.*, 2014, **100**, 166–178, DOI: **10.1016/j.carbpol.2012.12.043**.

47 M. Abrigo, S. L. McArthur and P. Kingshott, Electrospun nanofibers as dressings for chronic wound care: Advances, challenges, and future prospects, *Macromol. Biosci.*, 2014, **14**(6), 772–792, DOI: **10.1002/mabi.201300561**.

48 C. Madhusha, K. Rajapaksha, I. Munaweera, M. de Silva, C. Perera, G. Wijesinghe, *et al*, A novel green approach to synthesize curcuminoid-layered double hydroxide nanohybrids: Adroit biomaterials for future antimicrobial applications, *ACS Omega*, 2021, **6**(14), 9600–9608, DOI: **10.1021/acsomega.1c00151**.

49 K. L. Seneviratne, I. Munaweera, S. E. Peiris, C. N. Peiris and N. Kottegoda, Recent Progress in Visible-Light Active (VLA) TiO_2 Nano-Structures for Enhanced Photocatalytic Activity (PCA) and Antibacterial Properties: A Review, *Iran. J. Catal.*, 2021, 217–245.

50 P. Kodithuwakku, D. R. Jayasundara, I. Munaweera, R. Jayasinghe, T. Thoradeniya, M. Weerasekera, *et al*, A review on recent developments in structural modification of TiO_2 for food packaging applications, *Prog. Solid State Chem.*, 2022, **67**(100369), 100369.

51 S. Kumarage, I. Munaweera, C. Sandaruwan, L. Weerasinghe and N. Kottegoda, Electrospun amine-functionalized silica nanoparticles–cellulose acetate nanofiber membranes for effective removal of hardness and heavy metals (As(v), Cd(ii),Pb(ii)) in drinking water sources, *Environ. Sci.*, 2023, **9**(10), 2664–2679, DOI: **10.1039/d3ew00312d**.

52 S. D. Deshapriya and I. Munaweera, Visible-light-active electrospun membranes based on cobalt-doped ZnO nanohybrids: Applications for food packaging, *ChemistrySelect*, 2024, **9**(9), e202303830, DOI: **10.1002/slct.202303830**.

53 I. Munaweera and M. L. C. Madhusha, *Characterization Techniques for Nanomaterials*, CRC Press, Boca Raton, 2023.

54 I. Munaweera and M. L. Chamalki Madhusha, *Smart Nanomaterials*, CRC Press, London, England, 2023.

55 A. H. Uddin, R. S. Khalid, M. Alaama, A. M. Abdualkader, A. Kasmuri and S. A. Abbas, Comparative study of three digestion methods for elemental analysis in traditional medicine products using atomic absorption spectrometry, *J. Anal. Sci. Technol.*, 2016, **7**, 6, DOI: **10.1186/s40543-016-0085-6**.

56 R. López and R. Gómez, Band-gap energy estimation from diffuse reflectance measurements on sol–gel and commercial TiO2: a comparative study, *J. Solgel Sci. Technol.*, 2012, **61**(1), 1–7, DOI: **10.1007/s10971-011-2582-9**.

57 Z. Chen, J. Zhao, X. Yang, Q. Ye, K. Huang, C. Hou, *et al*, Fabrication of TiO_2/WO_3 composite nanofibers by electrospinning and photocatalystic performance of the resultant fabrics, *Ind. Eng. Chem. Res.*, 2016, **55**(1), 80–85, DOI: **10.1021/acs.iecr.5b03578**.

58 D. Sanna, G. Delogu, M. Mulas, M. Schirra and A. Fadda, Determination of free radical scavenging activity of plant extracts through DPPH assay: An EPR and UV–Vis study, *Food Anal. Methods*, 2012, **5**(4), 759–766, DOI: **10.1007/s12161-011-9306-1**.

59 CLSI, *Performance Standards for Antimicrobial Disk and Dilution Susceptibility Tests for Bacteria Isolated from Animals: Approved Standard: M31a2*, Clinical & Laboratory Standards Institute, 2nd edn, 2002, vol. 22, no.6.

60 **https://clsi.org/media/osthhxax/m27m44sed3e_sample.pdf**.

61 *M38Ed3 Filamentous Fungi antifungal susceptibility test [Internet]*, Clinical & Laboratory Standards Institute, [cited 2024 Mar 6], Available from: **https://clsi.org/standards/products/microbiology/documents/m38/**.

62 Z. You, X. Ran, Y. Dai and Y. Ran, Clioquinol, an alternative antimicrobial agent against common pathogenic microbe, *J. Mycol. Med.*, 2018, **28**(3), 492–501.

63 K. Amperayani, K. Naveen Kumar and U. Parimi, Synthesis and in vitro and in silico antimicrobial studies of novel piperine–pyridine analogs, *Res. Chem. Intermed.*, 2018, **44**(5), 3549–3564, DOI: **10.1007/s11164-018-3324-1**.

64 A. Naskar, S. Lee and K.-S. Kim, Easy One-Pot Low-Temperature Synthesized Ag-ZnO Nanoparticles and Their Activity Against Clinical Isolates of Methicillin-Resistant Staphylococcus aureus, *Front. Bioeng. Biotechnol.*, 2020, **8**, 216, DOI: **10.3389/fbioe.2020.00216**.

65 W. Purnamasari, T. A. Budiastanti, A. Aminatun, U. Rahmah, S. Sumarsih, J.-Y. Chang, *et al*, Naproxen release behaviour from graphene oxide/cellulose acetate composite nanofibers, *RSC Adv.*, 2022, **12**(13), 8019–8029, DOI: **10.1039/d1ra09293f**.

66 M. A. Teixeira, J. C. Antunes, C. L. Seabra, S. D. Tohidi, S. Reis, M. T. P. Amorim, *et al*, Tiger 17 and pexiganan as antimicrobial and hemostatic boosters of cellulose acetate-containing poly(vinyl alcohol) electrospun mats for potential wound care purposes, *Int. J. Biol. Macromol.*, 2022, **209**, 1526–1541, DOI: **10.1016/j.ijbiomac.2022.04.130**.

67 G. A. Bastida, R. J. Aguado, M. V. Galván, Z. MÁ, M. Delgado-Aguilar and Q. Tarrés, Impact of cellulose nanofibers on cellulose acetate membrane performance, *Cellulose*, 2024, **31**(4), 2221–2238, DOI: **10.1007/s10570-024-05760-9**.

68 R. Sinha, S. Janaswamy and A. Prasad, Enhancing mechanical properties of Electrospun Cellulose Acetate Fiber Mat upon Potassium Chloride exposure, *Materialia*, 2020, **14**(100881), 100881, DOI: **10.1016/j.mtla.2020.100881**.

69 Y.-S. Shin, M. Park, H.-Y. Kim, F.-L. Jin and S.-J. Park, Synthesis of silver-doped silica-complex nanoparticles for antibacterial materials, *Bull. Korean Chem. Soc.*, 2014, **35**(10), 2979–2984, DOI: **10.5012/bkcs.2014.35.10.2979**.

70 A. R. Zarei, A. Moloudi and S. G. Hosseini, Synthesis, characterization, and application of stabilized-Ni/Fe bimetallic nanoparticles for the selective elimination of chlorate impurity in military grade ammonium perchlorate, *Cent. Eur. J. Energ. Mater.*, 2017, **14**(1), 120–133, DOI: **10.22211/cejem/68391**.

71 M. Hafeez, R. Shaheen, B. Akram, H. S. Zain-ul-Abdin, S. Mahsud, *et al*, green synthesis of cobalt oxide nanoparticles for potential biological applications, *Mater. Res. Express*, 2020, **7**(2), 025019, DOI: **10.1088/2053-1591/ab70dd**.

72 J. Prakash, K. S. Venkataprasanna, G. Bharath, F. Banat, R. Niranjan and G. D. Venkatasubbu, In-vitro evaluation of electrospun cellulose acetate nanofiber containing Graphene oxide/TiO2/Curcumin for wound healing application, *Colloids Surf., A*, 2021, **627**(127166), 127166, DOI: **10.1016/j.colsurfa.2021.127166**.

73 C. Perruchot, M. A. Khan, A. Kamitsi, S. P. Armes, J. F. Watts, T. von Werne, *et al*, XPS characterisation of core–shell silica–polymer composite particles synthesised by atom transfer radical polymerisation in aqueous media, *Eur. Polym. J.*, 2004, **40**(9), 2129–2141, DOI: **10.1016/j.eurpolymj.2004.02.013**.

74 J. U. Kiran, J. P. Roners and S. Mathew, XPS and thermal studies of silver doped SiO2 matrices for plasmonic applications, *Mater. Today*, 2020, **33**, 1263–1267, DOI: **10.1016/j.matpr.2020.03.500**.

75 T. Ghodselahi, M. A. Vesaghi, A. Shafiekhani, A. Baghizadeh and M. Lameii, XPS study of the Cu@Cu2O core-shell nanoparticles, *Appl. Surf. Sci.*, 2008, **255**(5), 2730–2734, DOI: **10.1016/j.apsusc.2008.08.110**.

76 Q. M. Ahkam, E. U. Khan, J. Iqbal, A. Murtaza and M. T. Khan, Synthesis and characterization of cobalt-doped SiO2 nanoparticles, *Phys. B*, 2019, **572**, 161–167, DOI: **10.1016/j.physb.2019.07.044**.

77 I. Liakos, A. Holban, R. Carzino, S. Lauciello and A. Grumezescu, Electrospun fiber pads of cellulose acetate and essential oils with antimicrobial activity, *Nanomaterials*, 2017, **7**(4), 84, DOI: **10.3390/nano7040084**.

78 K. Garg and G. L. Bowlin, Electrospinning jets and nanofibrous structures, *Biomicrofluidics*, 2011, **5**(1), 13403, DOI: **10.1063/1.3567097**.

79 Y. Zheng, N. Meng and B. Xin, Effects of jet path on electrospun polystyrene fibers, *Polymers*, 2018, **10**(8), 842, DOI: **10.3390/polym10080842**.

80 A. Cimini, A. Borgioni, E. Passarini, C. Mancini, A. Proietti, L. Buccini, *et al*, Upscaling of Electrospinning technology and the application of functionalized PVDF-HFP@TiO2 electrospun nanofibers for the rapid photocatalytic deactivation of bacteria on advanced face masks, *Polymers*, 2023, **15**(23), 4586, DOI: **10.3390/polym15234586**.

81 M. A. Abdel Khalek, A. M. Abdelhameed and S. A. Abdel Gaber, The use of photoactive polymeric nanoparticles and nanofibers to generate a photodynamic-mediated antimicrobial effect, with a special emphasis on chronic wounds, *Pharmaceutics*, 2024, **16**(2), 229, DOI: **10.3390/pharmaceutics16020229**.

82 Y. Zhou, C. Jin, Y. Li and W. Shen, Dynamic behavior of metal nanoparticles for catalysis, *Nano Today*, 2018, **20**, 101–120, DOI: **10.1016/j.nantod.2018.04.005**.

83 P. Tzevelekidis, M. Theodosiou, A. Papadopoulou, E. Sakellis, N. Boukos, A. K. Bikogiannakis, *et al*, Visible-light-activated antibacterial and antipollutant properties of biocompatible Cu-doped and Ag-decorated TiO2 nanoparticles, *Heliyon*, 2024, **10**(17), e35634, DOI: **10.1016/j.heliyon.2024.e35634**; B. R. Cuenya, Synthesis and catalytic properties of metal nanoparticles: Size, shape, support, composition, and oxidation state effects, *Thin Solid Films*, 2010, **518**(12), 3127–3150, DOI: **10.1016/j.tsf.2010.01.018**.

84 M. Matalkeh, G. K. Nasrallah, F. M. Shurrab, E. S. Al-Absi, W. Mohammed, A. Elzatahry, *et al*, Visible light photocatalytic activity of Ag/WO3 nanoparticles and its antibacterial activity under ambient light and in the dark, *Results Eng.*, 2022, **13**(100313), 100313, DOI: **10.1016/j.rineng.2021.100313**.

85 E. Burello and A. P. Worth, A theoretical framework for predicting the oxidative stress potential of oxide nanoparticles, *Nanotoxicology*, 2011, **5**(2), 228–235, DOI: **10.3109/17435390.2010.502980**.

86 R. Borges, L. F. M. Amaral, T. J. Bondancia, R. A. de Freitas, F. Wypych and C. Ribeiro, Mechanochemical conversion of cellulose acetate from residues to cellulosic nanospheres for emulsion application, *J. Environ. Chem. Eng.*, 2023, **11**(3), 110119.

87 P. Shukla, A. K. Bajpai and R. Bajpai, Structural, morphological, thermal and mechanical characterization of cellulose acetate–poly (acrylonitrile) semi interpenetrating polymer network (IPN) membranes and study of their swelling behavior, *Polym. Bull.*, 2016, **73**(8), 2245–2264, DOI: **10.1007/s00289-016-1606-6**.

88 Z. Pang, R. Raudonis, B. R. Glick, T.-J. Lin and Z. Cheng, Antibiotic resistance in Pseudomonas aeruginosa: mechanisms and alternative therapeutic strategies, *Biotechnol. Adv.*, 2019, **37**(1), 177–192, DOI: **10.1016/j.biotechadv.2018.11.013**.

89 Y. Li, S. Kumar, L. Zhang and H. Wu, Klebsiella pneumonia and its antibiotic resistance: A bibliometric analysis, *BioMed Res. Int.*, 2022, **2022**, 1–10, DOI: **10.1155/2022/1668789**.

90 S. B. Kedare and R. P. Singh, Genesis and development of DPPH method of antioxidant assay, *J. Food Sci. Technol.*, 2011, **48**(4), 412–422, DOI: **10.1007/s13197-011-0251-1**.

91 D. Kaur and S. Chate, Study of antibiotic resistance pattern in methicillin resistant staphylococcus aureus with special reference to newer antibiotic, *J. Global Infect. Dis.*, 2015, **7**(2), 78, DOI: **10.4103/0974-777x.157245**.

92 D. Sengupta and A. Raghunathan, Rise of the superbugs: What we need to know: Overview of antimicrobial resistance, *Reson*, 2021, **26**(9), 1251–1266, DOI: **10.1007/s12045-021-1227-8**.

93 I. Munaweera and P. Yapa, *Principles and Applications of Nanotherapeutics*, CRC Press, Boca Raton, 2024.

94 Z. Shang, R. Wycisk and P. Pintauro, Electrospun composite proton-exchange and anion-exchange membranes for fuel cells, *Energies*, 2021, **14**(20), 6709, DOI: **10.3390/en14206709**.

95 B. Shmaefsky, Artificial urine for laboratory testing: Revisited, *Am Biol Teach*, 1995, **57**(7), 428–430, DOI: **10.2307/4450032**.

96 P. N. Yapa, I. Munaweera, M. M. Weerasekera and L. Weerasinghe, Nanoarchitectonics for synergistic activity of multimetallic nanohybrids as a possible approach for antimicrobial resistance (AMR), *JBIC, J. Biol. Inorg. Chem.*, 2024, **29**(5), 477–498, DOI: **10.1007/s00775-024-02066-w**.

97 M. Sethunga, M. M. K. D. Ranasinghe, K. K. D. S. Ranaweera, I. Munaweera and K. D. P. P. Gunathilake, Synergistic antimicrobial activity of essential oils and oleoresins of cinnamon (Cinnamomum zeylanicum), clove bud (Syzygium aromaticum) and ginger (Zingiber officinale), *Biocatal. Agric. Biotechnol.*, 2023, **51**, 102800, **https://www.sciencedirect.com/science/article/pii/S1878818123002013**.